Thesis for the Degree of Doctor of Philosophy

High-Resolution Spectroscopic Study of Giants and Supergiants using BOES: Exoplanet detection, Asteroseismology, and Spectral Atlas

Byeong-Cheol Lee

Department of Astronomy and Atmospheric Sciences
The Graduate School

June 2010

The Graduate School
Kyungpook National University

High-Resolution Spectroscopic Study of Giants and Supergiants using BOES: Exoplanet detection, Asteroseismology, and Spectral Atlas

Byeong-Cheol Lee

Department of Astronomy and Atmospheric Sciences
The Graduate School

Supervised by Professor Myeong-Gu Park and Inwoo Han

Approved as a qualified thesis of Byeong-Cheol Lee
for the degree of Doctor of Philosophy
by the Evaluation Committee

June 2010

Chairman Yong Hee Kang

Tae Seog Yoon

Kang – Min Kim

Inwoo Han

Myeong – Gu Park

The Graduate School Council, Kyungpook National University

Contents

List of Figures

List of Tables

Chapter 1

Introduction

1.1 Bohyunsan Observatory Echelle Spectrograph

1.1.1 Background and properties

In April 1996, Bohyunsan Optical Astronomy Observatory (BOAO) of Korea Astronomy & Space Science Institute (KASI) was opened with 1.8 m reflector. Photometric observations started at the end of that year while spectroscopic observations started in 2000 with Medium Dispersion Spectrograph (MDS). However, narrow wavelength range, low efficiency and bad opto-mechanics of the MDS made it difficult to carry out scientifically meaningful observations. The limitation in MDS's lifespan also made the problem worse. KASI began the developments of the Long Slit Spectrograph (LSS) and the Bohyunsan Observatory Echelle Spectrograph (BOES) in November 1996. These developments were completed in August 2003 (Kim et al. 2002, 2007). The BOES consists of three main parts; Cassegrain Interface Module (CIM), a light-transmitting fiber set, and a spectrometer. The BOES has several advantages as follows (Kim et al. 2007):

1) The wavelength coverage of the BOES is 3,500 $\sim$ 10,500 Å, which contains the whole visible and near infrared regions, distributed into $\sim$ 85 spectral orders. The attached CCD camera is equipped with 2K $\times$ 4K matrix (pixel size of 15μm $\times$ 15μm) which allows one to record the whole wavelength range in one exposure.

2) The BOES has five fibers of 80, 100, 150, 200, and 300 μm in diameter. The resolving power ($R = \lambda/\Delta\lambda$) of each fiber is 90,000, 75,000, 60,000, 45,000, and 30,000, respectively. In addition, two pairs of 150 and 200 μm fibers are available for spectropolarimetry with $R = \lambda/\Delta\lambda$ of 60,000 and 45,000.

3) The BOES is equipped with iodine (I_2) absorption cell needed for precise radial velocity (RV) measurements (see Chapter 1.4).

4) The maximum efficiency of the BOES is close to 12 % (for 300 μm in diameter) including the light loss due to the atmospheric extinction, the reflectance of the telescope, and the light cutoff at the fiber input (Kim et al. 2007). Compared to the efficiencies of other high-resolution spectrographs for $\sim$ 2 m class telescopes, $\sim$ 1 % of CES at Xinglong observatory (2.16 m telescope) in China (Jiang et. al. 1995), $\sim$ 2 % of HIDES at Okayama observatory (1.88 m telescope) in Japan (Izumiura et al. 1999), and $\sim$ 5 % of HES at Lick observatory (3 m telescope) in the USA (Vogt et al. 1999), the efficiency of the BOES is a lot better in the world.

1.1.2 Testing BOES with I_2 cell for RV stability

To demonstrate the stability of the BOES with I_2 cell, we observed long-term variations of a standard star, τ Ceti, and a binary star with a planetary companion τ Bootis. We obtained nightly observations of stars during 2003 and 2010 with 80 μm fiber. The BOES has been maintained at stable conditions for seven years with an actual accuracy of approximately 7 m s^{-1}.

1) τ Ceti

τ Ceti (G8 V, V = 3.5) has been known to be one of the most stable stars in RV measurements (Sato et al. 2002, Teixeira et al. 2009). We observed τ Ceti during November 2003 and January 2010 with 80 μm fiber and typical S/N ratios were $\sim$ 200 with exposure times of 3–10 min. As shown Figure 1.1, τ Ceti is measured with rms scatter of $\sim$ 6.7 m s^{-1}. Comparing the RV stabilities of the other spectrographs, the AAT Planet Search survey (Butler et al. 2001) shows constant RV at a level of $\sim$ 5 m s^{-1} and HIDES (Sato et al. 2002) at a level of 5.9 m s^{-1}.

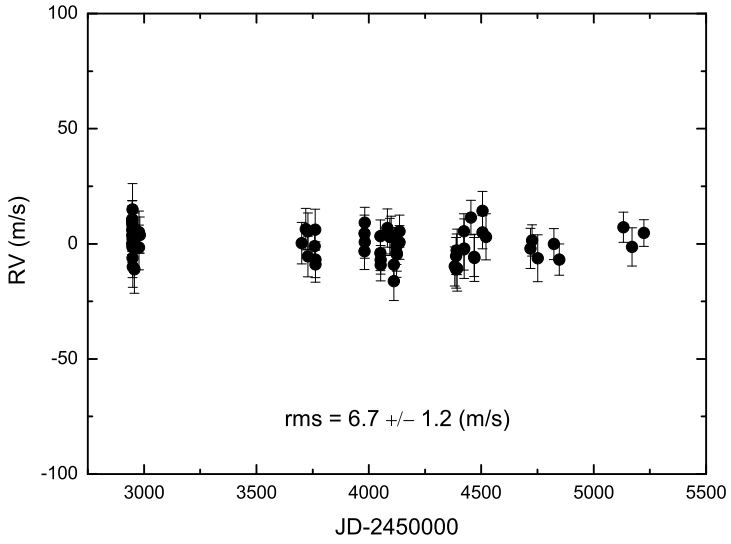

Figure 1.1: RV measurements of a standard star τ Ceti during November 2003 and January 2010.

2) τ Bootis

τ Boo (HD 120136; F6 IV, V = 4.5) is a yellow white dwarf with a red dwarf companion (M2 V, V=11.1). The primary star, τ Boo, is also known to have an extra-solar planet (exoplanet) called τ Boo b, showing an RV variation with the amplitude of 471 m s^{-1} and a period of 3.312 day (Butler et al. 1997, Fischer et al. 2001). We observed τ Boo with BOES on 63 separate nights during May 2003 and May 2010 (obtained total of 97 spectra). We used with 80 μm fiber and typical S/N ratios were $\sim$ 200 with exposure times of 10–15 min. Figure 1.2 plots the relative RV measurements for seven year observations. Analysis shows a period of 3.3126 days and a RV amplitude of 473 m s^{-1}. The eccentricity (e) of the orbit is 0.01 and the minimum mass of the companion is estimated to be 4.1 M_J (Jovian mass) with orbital radius of 0.05 AU. It is consistent with the result of Lick observatory (see Table 1.1). The rms residual from the orbital solution is as large as 50.6 m s^{-1}, which is caused by the binary companion. After removing the component due to the binary companion, the rms has decreased to 30 m s^{-1}. RV phase diagram for the orbit is shown in Figure 1.3.

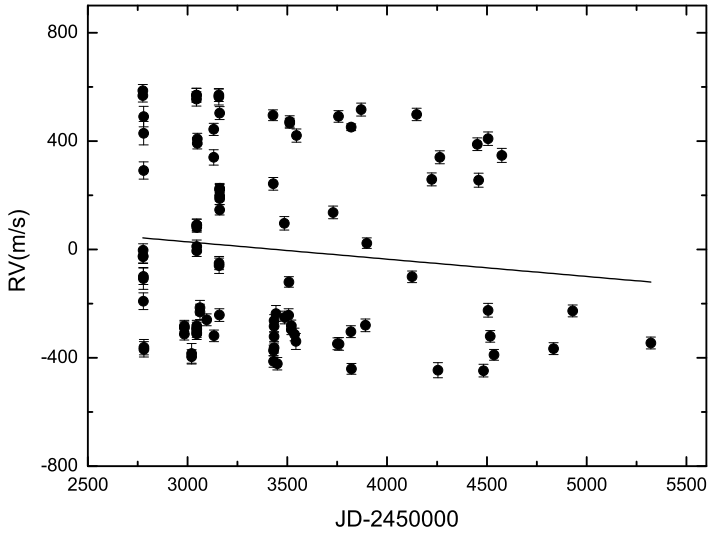

Figure 1.2: RV measurements of τ Boo during 2003 and 2010. The solid line shows the decline (–0.064 $\pm$ 0.004) of the orbital companion.

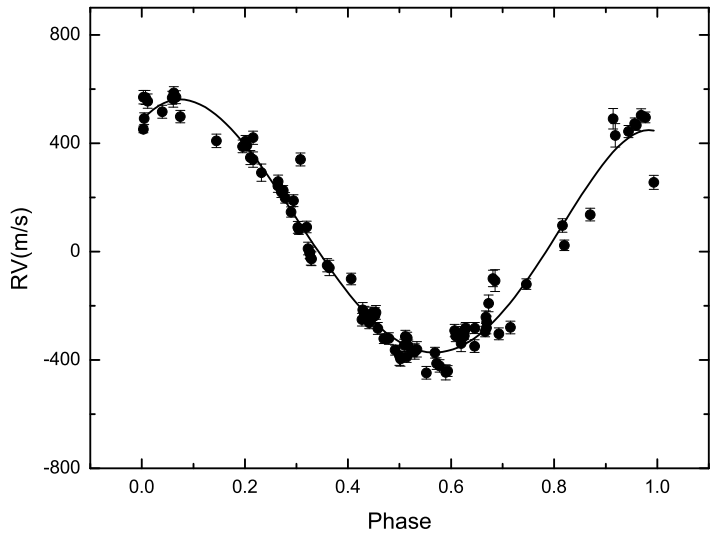

Figure 1.3: Phase curve of τ Boo with period of 3.312 days.

Table 1.1: Orbital parameters of the RV measurements for τ Boo b.

Parameter	Lick Obs.	BOAO	Unit
Period	3.313	3.312	[days]
$T_{\text{periastron}}$	2451622.28	—	[JD]
K	471.35	473.0	[m s^{-1}]
e	0.018	0.01	
ω	65.0	65.0	[deg]
$m \sin i$	4.13	4.10	[M_{Jup}]
a	0.05	0.05	[AU]
σ (O-C)	23.4	50.6	[m s^{-1}]

τ Boo is a visual binary, the projected separation of which has changed from 1849 to the recent. (10.3″ to 5.4″ by Gliese & Jahreiss 1979, 3.04″ by Kalas 2000, and 2.85″ by Lloyd et al. 2001). Since mid-1980s, τ Boo has been observed at Lick observatory and a shallow trend in the residual RV is apparent (Figure 1.4). Fit to the data shows a possible secondary companion with an orbital period longer than 20 yr and mass greater than 15 M_J. Except from 1987 to 1994 (internal errors at Lick observatory), RV has a linear slope of –15 m s^{-1} yr^{-1} with rms of 15.6 m s^{-1} (Fischer et al. 2001).

A long-term RV trend reported by Raghavan et al. (2006), which indicates the redetermination of the binary orbit, would be useful in τ Boo system. We compare the trend in the Lick observation with the BOES data. Linear fit to the BOES data shows a slope of –0.064 $\pm$ 0.004 for 7 years (Figure 1.2). It is consistent with the previous decline trend. We found a secondary orbital period of 7732 days (21.2 yr) and a RV amplitude of 191 m s^{-1}. It is estimated that the companion has the minimum mass of 22.1 M_J with orbital radius of 8.4 AU when the eccentricity is fixed at $e = 0$. The period of 21.2 yr is consistent with the expectation from the Lick observation. If the secondary RV of τ Boo continues to decline or change slowly, it should be determined within some years ahead to come.

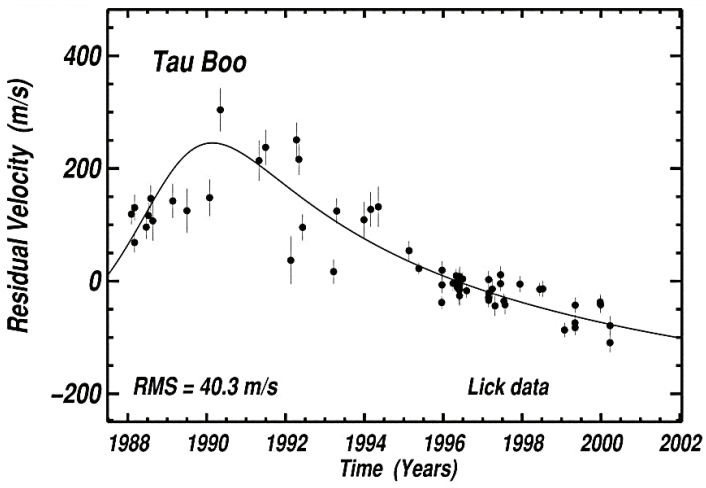

Figure 1.4: Residual velocities for τ Boo. The apparent variation is consistent with a companion in an orbital period longer than $\sim$20 yr and mass greater than $\sim$15M$_J$. It is possible that the nearly linear RV trend stems from a nearby M dwarf companion (Fischer et al. 2001).

1.2 Main research programs using BOES

Considering the moderate size of the telescope and not so good seeing condition at BOAO, the spectroscopic observation has a great advantage over showed some photometric one. As shown in the RV measurement precision (Kim et al. 2006), the BOES is quite competitive in the research fields of exoplanet detection and spectral atlas makings compared to the same class telescopes in the world.

1.2.1 Exoplanet detection and asteroseismology

In 1990s, a new field of astronomy called 'Search for extra-solar planets' was opened. Since the first discovery of an exoplanet (Mayor & Qulez 1995), more than 400 exoplanets have been detected. More than 80 % have been discovered by RV measurements and most of them were around solar-type main sequence stars. The first attempt to find exoplanets around giant stars such as α Boo (K1.5 III), β Gem (K0 IIIb), and α Tau (K5 III) was reported by Hatzes & Cochran (1993). The the last two stars recently showed some evidence that they have long-term variations due to companion (Hatzes et al. 2006, Reffert et al. 2006, and Hatzes et al. *in preparation*). Frink et al. (2002) discovered the first exoplanet around the K-giant star ι Dra (K2 III). Thereafter, several companions around giant stars have been found by the precise RV technique. Of $\sim$ fifty exoplanet search projects all over the world, about ten groups

including the BOAO possess both a high-resolution spectrograph and an analysis software. Along with exoplanet detection, another research field possible by the precise RV technique is asteroseismology, the science that studies the internal structure of stars through the interpretation of stellar pulsations. There are two exoplanet detection programs using BOES.

1) 'Exoplanet Detection and Asteroseismic Study of K-giants and Ap Stars' (Han et al. 2003) aims to clarify the nature and formation of planetary systems around intermediate-mass stars (A and F main sequence stars that are the progenitors of G- and K-giants), in the framework of international collaborations (Korea, Russia, Ukraine, Germany, and USA). The survey concentrates on chemically peculiar (Ap) stars and K-giants and supergiants. The details are explained in Section 1.3.

2) 'Search for Extrasolar Planets around G-type Giant Stars' (Sato et al. 2005) carries out a precise RV survey of late G-giants including early K-giants to search for exoplanets around intermediate-mass (1.5–5 $M_{\odot}$) stars. The studies of planetary systems around intermediate-mass stars are momentous issues because they convey important information on the planet formation mechanism. Its evolutionary time scale is very short, and proto-planetary disks also have short lifetimes to make planet. The existence of gas giant planets around such stars would constrain the timescale of giant planet formation and verify the current planet formation theory. Detecting planetary systems in intermediate-mass stars, however, is difficult because of broad and not so enough number of spec-

tral lines in early type main-sequence stars. On the other hand, G-giants are ideal targets for exoplanet detection around intermediate-mass stars because they have many sharp absorption lines suitable for precise RV measurements. This should help to understand a planet formation mechanism around intermediate-mass stars.

1.2.2 Spectral atlas

The analysis of high-resolution stellar spectra can reveal information about the physical conditions in the atmosphere, such as effective temperature, surface gravity and elemental abundances from the analysis of spectral lines. Spectral atlas provides the basic data needed for studies of stars, spectral classifications, stellar atmospheric models, and so on. Since the publication of the optical spectral atlas by Morgan et al. (1943), many spectral atlases covering a broad range in spectral and luminosity classes have been published. However, most existing atlases are of low or medium spectral resolution. Recently, with the introduction of high-resolution spectrographs, several spectral high-resolution atlases with extremely high S/N rations have been published: an atlas of HD 175640 (B9 III) in the region from 3040 to 10,000 Å (Castelli & Hubrig 2004), an atlas of o Peg (A1 IV) in the region from 3826 to 4882 Å (Gulliver et al. 2004), an atlas of Deneb (A2 Ia) in the region from 3826 to 5212 Å (Albayrak et al. 2003), and an atlas of Arcturus (K2 IIIp) in the region from 3727 to 9300 Å (Hinkle et al. 2000). Still more high-resolution

spectral atlases are needed. There are two kinds of spectral atlas and abundance analysis projects using BOES.

1) 'High-resolution spectral atlases of bright stars' (Kim et al. 2005) aims to develop spectral atlases with high resolution (R $\sim$ 90,000) and high S/N ratio ($\sim$ 1000) for bright stars of the various spectral classes. The atlases produced will be a fundamental reference source in stellar spectroscopy. The complete atlases with line identifications will be presented in digital form and available online. Accurate and basic physical parameters for each object will also be determined and appropriate synthetic spectra will be calculated and presented as well. The details are in Section 1.3.

2) 'Abundance determinations on an unbiased sample of late-B through A stars within 50 pc' (Takeda et al. 2007) aims to study the chemical properties of their unevolved counterparts (late B and A-type stars on the upper main sequence, in order to understand the abundance characteristics of late G through early K-giants. Unfortunately, current published abundance studies on these objects are severely "biased" toward sharp-line stars. Considering thus the necessity of abundance information on an "unbiased" sample of such early type stars, spectroscopic observations of these stars using BOES are needed, with a wide wavelength coverage at one exposure.

1.3 Program stars

1) For exoplanet detection and asteroseismology by precise RV measurements, early type stars (O-, B-, and A-type) are unfavorable because of their broad spectral line widths and scarcity of spectral lines. In case of F-, G-, and K-dwarfs, they have a decided advantage that they usually have many sharp absorption lines in their spectra while the stars themselves remain relatively stable against pulsations and surface activities. Since the beginning of 1990s, the main-sequence stars already have been surveyed for exoplanet detection in many observatories such as Lick observatory, McDonald observatory, European Southern Observatory (ESO), therefore the BOES does not have any special advantages as far as these stars are concerned.

Giants and supergiants, massive stars in evolved stages, are also promising targets for exoplanet detection because they usually have more sharp absorption lines than F-, G-, and K-dwarfs. On the other hand, the stars themselves are relatively unstable, showing pulsations and surface activities. In same cases, thus, both exoplanet detection and asteroseismic investigation could be complementary to each other. Since 2001, Sato et al. already has been carrying out a precise RV survey of 300 late G-giants to search for exoplanets around intermediate-mass stars at Okayama Astrophysical Observatory (OAO) in Japan.

Accordingly, we selected early and bright 55 K-giants and supergiants

(and several F- and M-giants and supergiants) to avoid overlap with other programs, which are thus ideal targets for exoplanet detection around intermediate-mass stars (Appendix B). And, to include a significant sample of A-, and F-type main-sequence stars that are the progenitors of G- and K-giants, we add 30 chemically peculiar (Ap) stars (Appendix B). Because Ap stars have slower rotation rates than their normal counterparts and they are overabundant in Si, Cr, and rare earths, their spectra reveal narrow and many spectral lines respectively. These abundances can be as high as 10,000 times solar values. So, in spite of being early type stars Ap stars have a plethora of narrow spectral lines which are amenable to RV measurements. The asteroseismic investigations of pulsating Ap stars from our sample will be undertaken to study the structure and surface anomalies. The results of this survey may provide clues to the role of stellar mass in the process of planet formation and pulsational instability among the K-giants and supergiants.

2) We select stars with various spectral classes, O through M-type as well as dwarf through supergiant, because we want to avoid a biased sample and show a balanced statistics. Fifty bright stars were selected after checking interstellar extinction of E(B–V) < 0.1 (Appendix B). Each of them provides the basic data needed for studies such as peculiar stars, composite systems (multiple systems, stellar clusters, and galaxies), spectral classifications, testing model stellar atmospheres, and interstellar extinctions by dust.

1.4 Description of precise RV measurement

Because wavelength reference is taken at a different time and often traverses a different light path with a stellar spectrum, traditional RV measurement techniques rarely exceed a precision of $200 \sim 500$ m s^{-1} (Kürster et al 1994). Using RV standard star can avoid the problem of different light paths for the reference and stellar spectra. But, the standard star is still observed at a different time and it is doubtful of small stellar oscillations. This instrumental problem can be overcome by superimposing the wavelength reference and stellar spectrum. Thus, instrumental shifts affect both the wavelength reference and stellar spectrum equally.

Griffin and Griffin (1973) first proposed using telluric O_2 lines at 6300 Å as an RV reference. This technique was used widely at McDonald observatory in a planet search program and a long-term stability with precision of $15 \sim 20$ m s^{-1} (Cochran and Hatzes 1990). But, this is still influenced by pressure and temperature changes of the atmosphere condition.

Subsequently improved technique was developed using a gas cell inside which pressure and temperature can be regulated. Precise RV technique with the HF (Hydrogen Fluoride) absorption cell was developed by Campbell et al. (1979, 1988). Approximately 20 m s^{-1} RV precision can be obtain using HF cell, but it didn't continue due to noxiousness, short wavelength scale ($\sim$ 100 Å), high heating temperature ($\sim$ 100 °C), and

big instrumental size. Marcy & Butler (1992) substituted an iodine (I_2) cell for the HF cell. It has several great advantages: wide wavelength region (5000 $\sim$ 6300 Å), no-high heating temperature ($\sim$ 67 °C), small size of a cell, and innoxiousness.

Kim et al. (2002) developed an I_2 cell system attached to the BOES on 1.8 m telescope for precise stellar RV measurements. The modeling technique is similar to that described by Marcy & Butler (1992), Valenti et al. (1995), Butler et al. (1996), and Endl et al.(2000). An I_2 cell is placed at the front of the slit assembly.

An I_2 cell has robust lines that are convolved to the original spectra, which are very difficult to de-convolve the original. The stellar spectrum taken through I_2 cell is modeled as the product of high-resolution stellar and I_2 template spectra convolved with the modeled instrumental profile (IP) of the spectrograph. In other to determine the stellar RV measurements, Han et al. (2007) construct a parameterized model for a star with I_2 spectrum. A spectrum taken through the I_2 cell, $I(\lambda)$, can be modeled using two functions, the intrinsic stellar spectrum (template spectrum), $S(\lambda)$, and the transmission function of the I_2 cell, $A(\lambda)$, as

$$I(\lambda) = k\ [A(\lambda)\ S(\lambda + \Delta\lambda)] * \mathrm{IP},$$

where, k is a normalization factor, $\Delta\lambda$ is the Doppler shift, IP is the instrumental profile, and "$*$" represents convolution. The $A(\lambda)$ and $S(\lambda)$ are normalized with respect to their continuum levels.

As $A(\lambda)$, the BOES use the Lick-Hamilton I_2 cell spectrum of extremely high-resolution (R $\sim$ 400,000) spectrum, which was obtained by the Fourier Transform Spectrometer of Kitt Peak National Observatory. To obtain the $S(\lambda)$, we need the following processing. A template stellar spectrum (without I_2 cell) should be obtained with high-resolution and not be smeared by the IP of the spectrograph. And, Han et al. (2007) obtain a convolved spectrum by IP, which is a Tungsten Halogen Lamp (THL) spectrum go though the I_2 cell. With previous two spectra, they get the IP under each chunk and template spectrum. Previous two spectra should have high-resolution and not be smeared by the IP of the spectrograph. For the IP modeling, the technique described by Valenti et al. (1995) was adopted. This is modeled with a combination of a central and several satellite Gaussian profiles which are placed at appropriate intervals and have suitable widths, depending on the properties of the spectrograph.

With this description, Han et al. (2007) developed the I_2 cell analysis software (RVI2CELL). It adopts basically the same algorithm and procedures described by Marcy & Butler (1992). However, the IP model using the matrix formula described by Endl et al. (2000) was used. The solution of the matrix equation using singular value decomposition instead of the maximum entropy method by Endl et al. (2000) was adopted. With this configuration, RVI2CELL achieved a typical internal RV accuracy of $\sim$10 m s^{-1} depending on a quality of a spectra. RV precision tests with

RVI2CELL were shown in Section 1.1.2. For all our relevant analysis, we used RVI2CELL.

1.5 The aims of this thesis

After development of a high-resolution echelle spectrograph, the BOES in 2003, two main research programs of exoplanet detections and making spectral atlases of giants and supergiants have been carrying out. Through the program 'Exoplanet Detection and Asteroseismic Study of K-giants and Ap Stars', we have performed precise RV measurements of Polaris (F7 Ib) and α Arietis (K2 III). They did not reveal well for a nature and a cause of those stars such as RV variations, oscillations, surface feature and companion. And, we make a high quality spectral atlas of α Persei under the program 'High-resolution spectral atlases of bright stars' and provide identifications of spectral features with a high S/N ratio and a wide wavelength region.

The aim of this thesis is as follows; 1) Verification of an accuracy of the BOES RV measurements, 2) Report on periodic RV variations observed in giants and supergiants, and attempt to reveal the nature of these variations, and 3) Making a high-resolution spectral atlas of supergiant.

A background of the BOES, procedures of a testing BOES RV stability, justification of program stars, and description of a precise RV

measurement are already described in this Chapter. The three program stars are used for the thesis. A high-resolution spectral atlas of α Persei is presented in Chapter 2. Precise RV measurements of Polaris and α Arietis are discussed in Chapter 3 and 4. A summary of the thesis is given in Chapter 5. Appendix A contains whole spectral atlas, synthetic spectrum, and line tables and figures. Appendix B shows the list of program stars. RV measurements of Polaris and α Arietis list in Appendix C. And Appendix D is list of SCI papers using BOES.

References

Artymowicz, P., & Lubow, S. H. 1994, ApJ, 421, 651

Butler, R. P., Marcy, G. W., Williams, E., McCarthy, C., Dosanjh, P., & Vogt, S. S. 1996, PASP, 108, 500

Butler, R. P., Marcy, G. W., Williams, E., Hauser, H., & Shirts, P. 1997, ApJL, 474, L115

Butler, R. P., Tinney, C. G., Marcy, G. W., Jones, H. R. A., Penny, A. J., & Apps, K. 2001, ApJ, 555, 410

Campbell, B., & Walker, G. A. H. 1979, PASP, 91, 540

Campbell, B., Walker, G. A. H., & Yang, S. 1988, ApJ, 331, 902

Castelli, F., & Hubrig, S. 2004, A&A, 425, 263

Cochran, W. D., & Hatzes, A. P. 1990, BAAS, 22, 1082

Endl, M., Kürster, M., & Els, S. 2000, A&A, 362, 585

Fischer, D. A., Marcy, G. W., Butler, R. P., Vogt, S. S., Frink, S., & Apps, K. 2001, ApJ, 551, 1107

Frink, S., Mitchell, D. S., Quirrenbach, A., Fischer, D. A., Marcy, G. W., & Butler, R. P. 2002, ApJ, 576, 478

Gliese, W., & Jahreiß, H. 1979, A&AS, 38, 423

Griffin, R., & Griffin, R. 1973, MNRAS, 162, 255

Gulliver, A. F., Adelman, S. J., & Friesen, T. P. 2004, A&A, 413, 285

Han, I., Kim, K.-M., Lee, B.-C., & Valyavin, G. 2007, Publication of Korean Astronomical Society, 22, 75

Hatzes, A. P., & Cochran, W. D. 1993, ApJ, 413, 339

Hatzes, A. P., Cochran, W. D., Endl, M., Guenther, E. W., Saar, S. H., Walker, G. A. H., Yang, S., Hartmann, M., Esposito, M., Paulson, D.

B., & Dollinger, M. P. 2006, A&A, 457, 335

Hatzes, A. P. Guenther, E. W., Zechmeister, M., Dollinger, M., Cochran, W. D., Hartmann, M., Esposito, M., Walker, G. A. H., Yang, S., Han, I., Lee, B.-C., Kim, K.-M., Mkrtichian, D., and Girardi, L. *in preparation*

Hinkle, K., Wallace, L., Valenti, J., & Harmer, D. 2000, ISBN: 1-58381-037-4, 2000

Izumiura, H. 1999, http://www.oao.nao.ac.jp/en/telescope/

Jiang, S. H. 1995, "The Double Beam Echelle Spectrograph of the 2.16 m Telescope of Beijing Astronomical Observatory", p335, pub. by NAOJ.

Kalas, P. 2000, From Extrasolar Planets to Cosmology: The VLT Opening Symposium, 415

Kim, K-M., Jang, B.-H., Han, I., Jang, J. G., Sung, H. C., Chun, M.-Y., Hyung, S., Yoon, T.-S., & Vogt, S. S. 2002, Journal of Korean Astronomical Society, 35, 221

Kim, K. M., Mkrtichian, D. E., Lee, B.-C., Han, I., & Hatzes, A. P. 2006, A&A, 454, 839

Kim, K.-M., Han, I., Valyavin, G. G., Plachinda, S., Jang, J. G., Jang, B.-H., Seong, H. C., Lee, B.-C., Kang, D.-I., Park, B.-G., Yoon, T. S., & Vogt, S. S. 2007, PASP, 119, 1052

Kürster, M., Hatzes, A. P., Cochran, W. D., Pulliam, C. E., Dennerl, K., & Döbereiner, S. 1994, The Messenger, 76, 51

Lloyd, J. P., Liu, M. C., Graham, J. R., Enoch, M., Kalas, P., Marcy, G. W., Fischer, D., Patience, J., Macintosh, B., Gavel, D. T., Olivier, S. S., Max, C. E., White, R., Ghez, A. M., & McLean, I. S. 2001, arXiv:astro-ph/0103027

Marcy, G. W., & Butler, R. P. 1992, PASP, 104, 270

Mayor, M., & Queloz, D. 1995, Nature, 378, 355

Morgan, W. W., Keenan, P. C., & Kellman, E. 1943, Science, 97, 536

Raghavan, D., Henry, T. J., Mason, B. D., Subasavage, J. P., Jao, W.-C., Beaulieu, T. D., & Hambly, N. C. 2006, ApJ, 646, 523

Reffert, S., Quirrenbach, A., Mitchell, D. S., Albrecht, S., Hekker, S., Fischer, D. A., Marcy, G. W., & Butler, R. P. 2006, ApJ, 652, 661

Sato, B., Kambe, E., Takeda, Y., Izumiura, H., & Ando, H. 2002, PASJ, 54, 873

Teixeira, T. C., Kjeldsen, H., Bedding, T. R., Bouchy, F., Christensen-Dalsgaard, J., Cunha, M. S., Dall, T., Frandsen, S., Karoff, C., Monteiro, M. J. P. F. G., & Pijpers, F. P. 2009, A&A, 494, 237

Valenti, J. A., Butler, R. P., & Marcy, G. W. 1995, PASP, 107, 966

Vogt, S. S. 1999, "Phase B Report of the BOES", BOAO

Chapter 2

A High-Resolution Spectral Atlas of α Persei from 3810 to 8100 Å

Abstract[1]

We present a high resolution ($\lambda/\delta\lambda$ = 90,000) spectral atlas of the F5 Ib star α Per covering the 3810 – 8100 Å region. The atlas, based on data obtained with the aid of the echelle spectrograph BOES fed by 1.8 m telescope at Bohyunsan observatory (Korea), is a result of co-addition of a few well-exposed spectra. The final signal-to-noise ratio is ∼800 at ∼6000 Å. The atlas is compared with a synthetic spectrum computed using a code based on Kurucz software and databases. The adopted model atmosphere parameters are $T_{\rm eff}$ = 6240 ± 20 K, log g = 0.58 ± 0.04, and $v_{\rm micro}$ = 3.20 ± 0.05 km s^{-1}. We also derived an iron abundance of [Fe/H] = –0.28 ± 0.06. The spectral lines of α Per have been identified by matching the synthetic spectrum with the observed one. The atlas is presented in figures and available in digital form on the World Wide Web, along with synthetic spectrum and spectral line identification tables.

[1]Chapter 2 is published in the April 2006 issue of *The Publications of the Astronomical Society of the Pacific*, Vol. 118: 636-641

2.1 Introduction

Since the publication of the optical spectral atlas by Morgan & Kellman (1943), many stellar spectral atlases covering a broad range in spectral and luminosity classes have been published. Spectral atlases provide the basic data needed for studies of peculiar stars and composite systems (multiple systems, stellar clusters, and galaxies), automated spectral classification, testing of stellar atmospheric models, and so forth. However, most existing atlases are of low or medium spectral resolution.

Recently, several high-resolution (R $\geq$ 90,000) and extremely high signal-to-noise ratio (S/N) spectral atlases have been published: an atlas of HD 175640 (B9 III) in the region from 3040 to 10,000 Å (Castelli & Hubrig 2004), an atlas of o Peg (A1 IV) in the region from 3826 to 4882 Å (Gulliver et al. 2004), an atlas of Deneb (A2 Ia) in the region from 3826 to 5212 Å (Albayrak et al. 2003), and an atlas of Arcturus (K2 IIIp) in the region from 3727 to 9300 Å (Hinkle et al. 2000). One of the most popular and widely used spectral atlases is the solar atlas in the region from 2960 to 13,000 Å by Kurucz et al (1984).

In this paper we present a high-resolution, high S/N atlas of α Per, the brightest star in the well-studied cluster of the same name. The star α Persei (33 Persei, HD 20902, HR 1017, SAO 38787, HIP 15863) is a well-studied F-type supergiant with sharp-lined features. It is slightly reddened [E$(B-V) = 0.04$; Gray 1991] object with weak longitudinal

magnetic fields of $B_l = 1 \pm 2$ G (Shorlin et al. 2002). Such small magnetic fields allow us to neglect the Zeeman splitting effect in calculations of synthetic spectra. More detailed information about the star can be found in Evans et al (1996).

The aim of this article is to present a high-quality atlas of α Per and to provide identification of spectral features. A detailed abundance analysis will be presented in a separate publication.

2.2 Observations and data reduction

High-resolution spectra of α Per have been acquired using the Bohyunsan echelle spectrograph (BOES) [2] fed by the 1.8 m telescope of Bohyunsan Optical Astronomy Observatory in Korea. The spectra were recorded during several observing runs in the period from 2004 October to 2005 March (see Table 1). The spectrograph has three observational modes with resolving powers of 30,000, 45,000, and 90,000. Our spectra were obtained at the highest resolution. The spectrograph allows us to cover in a single exposure the wavelength range from ∼3700 to ∼10,000 Å, divided into ∼80 spectral orders with a CCD camera equipped with a 4096×2048 pixel matrix (pixel size 15 μm × 15 μm). The achieved resolution allows precise measurements of the wavelengths and intensities of stellar and interstellar features.

[2] A detailed description of the spectrograph is given at http://www.boao.re.kr/BOES/BOESppt3.files/frame.htm.

Table 2.1: List of α Persei spectra.

Date	Number of spectra	HJD[a]	Divisor	S/N ∼3900 Å	S/N ∼6000 Å	S/N ∼8100 Å
2004 Oct. 20	5	2453299.14037	HD 218045	75	350	245
2004 Nov. 21	20	2453331.16379	HD 218045	65	260	250
2004 Nov. 22	22	2453332.11928	HD 218045	80	270	260
2004 Nov. 23	23	2453333.26396	HD 120315	70	250	245
2004 Dec. 13	20	2453353.13167	HD 218045	110	450	380
2005 Mar. 13	4	2453442.98274	HD 87901	90	320	230
2005 Mar. 14	4	2453443.98124	HD 87901	70	300	220
2005 Mar. 20	4	2453449.95428	HD 120315	65	280	210

[a] Heliocentric Julian Date of midpoint of the exposure

All the observed spectra are listed in Tables 2.1, where the Heliocentric Julian Date of the middle of exposure, number of object frames, name of object, spectrum used for telluric line removal, and estimated S/Ns in three wavelength regions from blue to red are given.

Our reduction of the echelle spectra was performed using both the IRAF (Tody 1986) and the DECH (Galazutdinov 1992). The programs allowed us to perform all of the standard procedures for CCD spectra processing and analyzing. The wavelength scale was constructed on the basis of a global polynomial of the form described in detail in Galazutdinov et al. (2000). IRAF was used for image processing and the extraction of spectra from two-dimensional images. Further data processing and analysis were performed using the DECH code.

Data processing was performed in several steps. The first one was telluric line removal. Each original α Per spectrum is blended with telluric lines at wavelengths longer than $\sim$5800 Å. To eliminate them, we specially recorded spectra of so-called divisors, hot and rapidly rotating stars without reddening that allow to remove telluric lines: HD 87901 (α Leo; B7 V), HD 120315 (η UMa; B3 V), and HD 218045 (α Peg; B9.5 III). Before division, all stellar lines seen in the spectra of the divisors were eliminated using normalization by a pseudocontinuum. Figure 2.1 demonstrates the effect of the telluric line removal procedure. However, in the strong telluric lines, it is difficult to remove them completely, as is seen in two wavelength ranges: 6868–6940 and 7594–7652 Å.

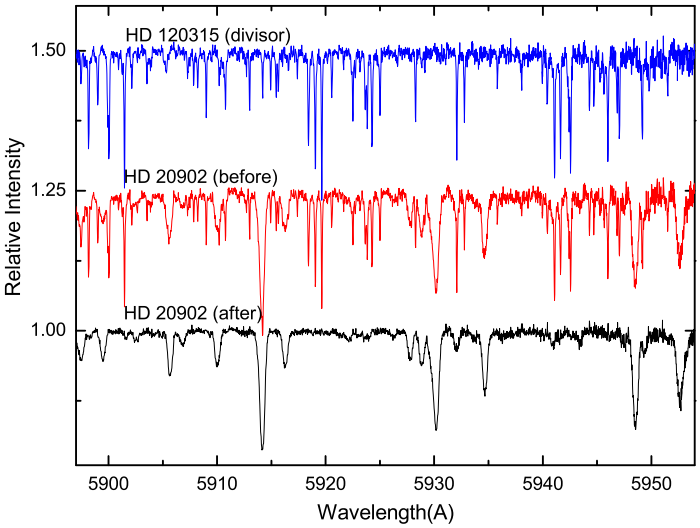

Figure 2.1: Demonstration of telluric line removal. *Top to bottom*: Divisor (HD 120315), original spectrum of α Persei, and resulting spectrum after telluric lines are divided out.

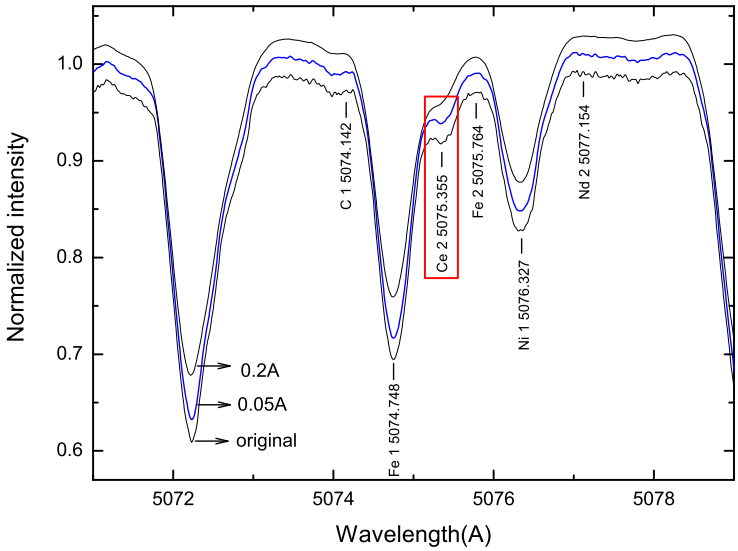

Figure 2.2: A demonstration of smoothing procedure. The original spectrum (*bottom*) is shown together with convolved ones. The top and middle spectra are the results of convolutions with Gaussian profiles of 0.2 and 0.05 ÅFWHM, respectively. Note the Ce II (5075.355 Å) profile behavior. Excessive convolution (*top*) leads to profile degradation.

To improve the S/N of the final spectrum, we combined all spectra of α Per listed in Table 2.1. Before co-adding, the wavelength scale of each individual spectrum was shifted to the rest-wavelength velocity frame. This allows the co-addition of the reduced spectra, which increases the S/N of the final spectrum by up to ∼800 at ∼6000 Å.

The co-added spectrum was finally smoothed to remove high-frequency noise patterns. For smoothing we applied convolution with a Gaussian profile. To avoid degradation of the spectral resolution, we adopted individually the full width at half-maximum (FWHM) of the Gaussian profile for each spectral order. The final FWHM is 2.3 pixels, which corresponds to 0.044–0.09 Å according to the linear dispersion of the corresponding spectral orders, which range from 0.019 Å pix^{-1} (at 3810 Å) to 0.039 Å pix^{-1} (at 8100 Å). In Figure 2.2 we demonstrate the effect of the smoothing procedures. As one can see, smoothing with the chosen profiles increases the S/N by up to 40% without loss of spectral resolution.

The last procedure that we have applied is refining the continuum position using the synthetic spectrum described below. An example of the final spectrum is shown in Figure 2.3. For clarity, each piece of the spectrum is shown twice in a single panel with different scales: one is shown on the entire intensity scale, while the other is shown with a magnification factor of 20. The idea of such figures is to make possible the detailed examination of weak lines profiles.

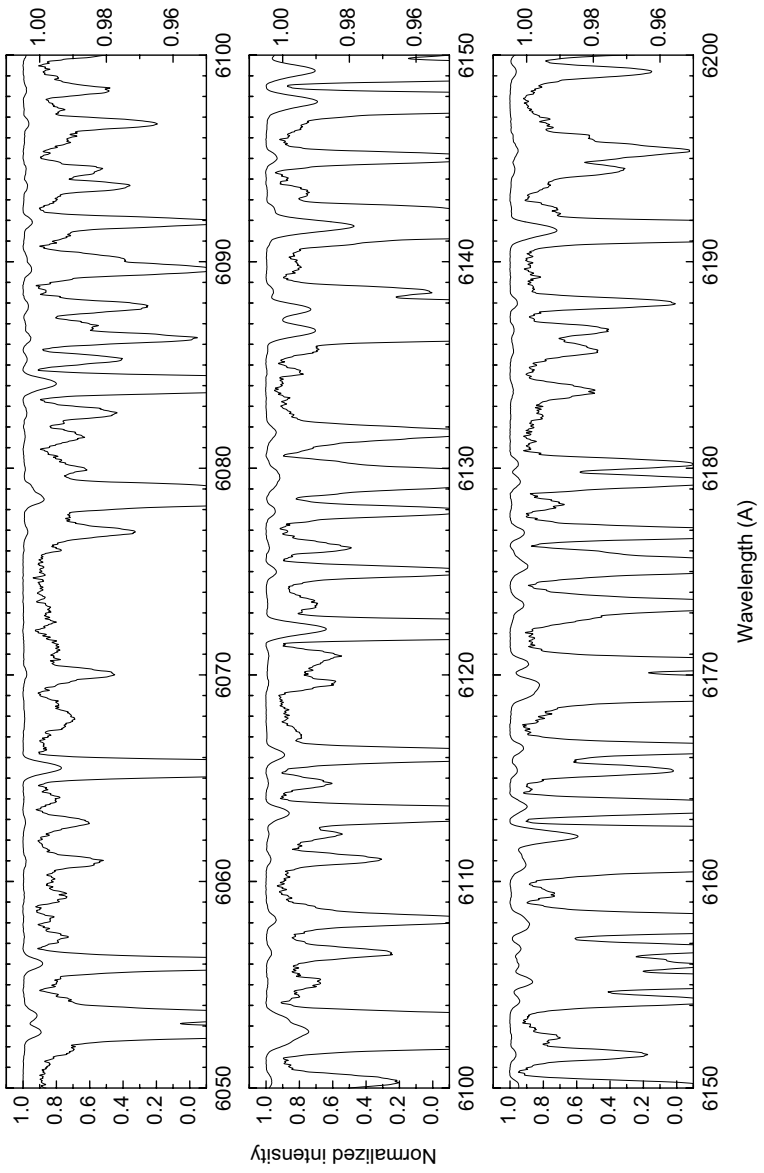

Figure 2.3: Example of spectral atlas of α Per.

The complete atlas of α Per can be downloaded from the Internet[3], along with the synthetic spectrum and line identification tables.

2.3 Atmosphere parameters and metallicity

The atmosphere parameters of α Per vary from author to author, as shown in a detailed study by Evans et al. (1996). Here we list the basic physical parameters of α Per determined by different methods in the relatively recent literature.

- Using *IUE* (*International Ultraviolet Explorer*) spectra, $BVRIJK$ photometry, and model atmosphere methods, Evans et al (1996) found an effective temperature $T_{\rm eff}$= 6270 K. (The surface gravity and microturbulent velocity were fixed at log g= 1.5 and $v_{\rm micro}$= 4 km s^{-1}, respectively.)

- Andrievsky et al. (2002) estimated the physical parameters of the star as follows: $T_{\rm eff}$= 6200 K, log g= 0.7, [Fe/H]= –0.2, and $v_{\rm micro}$= 2.9 km s^{-1}. They used several broadband photometric calibrations and high-resolution spectra.

- Takeda & Takata-Hidai (1995, 1998, 2000) reported abundances of light elements in the atmosphere of α Per and used somewhat

[3]See http://www.boao.re.kr/BOES/atlas/hd20902.html; also available at http://vizier.u-strasbg.fr.

different physical parameters: $T_{\rm eff}$= 6250 K, log g= 0.9, [Fe/H]= +0.03, and $v_{\rm micro}$= 4 km s^{-1}.

We also made several attempts to determine the basic parameters of α Per. First, using the Geneva system photometric data taken from the SIMBAD database and the calibration of Kunzli et al. (1997), we found that $T_{\rm eff}$= 5967 K, log g= 0.71, and [Fe/H]= –0.29. Second, using several sources described below, we constructed a mean energy distribution of α Per and fitted it with the Kurucz (1993) fluxes. For this task we calculated the mean spectral energy distribution in UV range using several *IUE* exposures[4] taken from the INES database. In the visible band, the observed energy distributions were constructed using the catalogs III/201 (Alekseeva et al. 1997), III/202 (Kharitonov et al. 1988), and III/208 (Glushneva et al. 1984) from the SIMBAD database. A $JKLMN$ photometry data from SIMBAD and *IRAS Infrared Astronomical Satellite* fluxes were used as well. Using all these observations, we interpolated the Kurucz fluxes and found the best fit with the following parameters: $T_{\rm eff}$= 6005 ± 50 K, log g= 0.00, and [Fe/H]= –0.08 ± 0.05 in the E($B-V$) range from 0.00 to 0.06.

Thus, the effective temperature of α Per determined by different methods lies in the range ∼5967–6270 K. However, there are direct

[4]Namely: LWP02909RS, LWP03009RS, LWR03027RS, LWR03102RS, LWR03293RS, LWR03294RS, LWR04227RS, LWR04228RS, LWR05780RS, LWR09992RL, LWR11329RS, LWR11330RS, LWR12715RS

measurements of the angular diameter of α Per by Nordgren et al. (2001) and Mozurkewich et al. (2003). The latter work gives values from 2.79 to 3.06 mas for the angular diameter of uniform-brightness disk at different wavelengths and 3.188 $\pm$ 0.0035 mas for a limb-darkened disk. Using infrared flux method, Mozurkewich et al. (2003) estimated a temperature $T_{\rm eff}$= 6750 $\pm$ 85 K. It should be noted that temperatures of supergiants by Mozurkewich et al. (2003) are not compatible with observed V–K colors, and these authors pointed out that a possible reason for this discrepancy is poor extinction correction.

Therefore, we decided to determine the physical parameters of α Per directly from the spectrum. As a first step, we adopted the atmospheric parameters of the star derived by Andrievsky et al. (2002). These parameters were used to find the continuum level and to identify the unblended iron lines in the spectrum. The equivalent widths of these lines were used to find more precise values of the above-mentioned parameters and microturbulent velocity. After that, we refined the parameters using the method described by Yushchenko (1998) and Gopka et al. (2004), which is based on the calculation of iron abundances for a set of models with different temperatures (from 5875 to 7250 K with a step size of 125 K), surface gravities (log g= 0.5 – 2.0 with a step size of 0.1) and microturbulent velocities (from 0.1 to 9.9 km s^{-1}). For each model we analyzed the behavior of abundance of individual lines, such as its dependence on their equivalent widths and the energy of the low-level transition. The

rms errors of the mean iron abundance were taken into account as well. In the end, we strove to find the values of $T_{\rm eff}$, log g, and $v_{\rm micro}$that provide (1) the coincidence of neutral and ionized iron abundances and (2) the independence of abundances of individual lines from equivalent widths and the low-level energy.

Abundances were calculated with the WIDTH9 code of Kurucz (1993) using the equivalent widths of 71 lines of neutral and 34 lines of ionized iron. Oscillator strength of lines were taken mainly from Kurucz (1993) and Hirata & Horaguchi (1995; SIMBAD catalog VI/69). A comparison of the solar atlas (Dellbouille et al. 1973) with synthetic solar spectrum calculated with the aid of the Kurucz (1993) SYNTHE and Yushchenko et al. (1999) URAN codes allowed us to estimate the solar oscillator strengths for some of the lines.

The last iteration was made using a set of models of [Fe/H]= – 0.3 with $T_{\rm eff}$ from 6000 K to 6400 K (10 K steps) and surface gravities from log g= 0.3 to 0.9 (0.02 dex steps). Finally, we found an iron abundance of [Fe/H]= – 0.28 ± 0.06 for the following parameters: $T_{\rm eff}$= 6240 ± 20 K, log g= 0.58 ± 0.04, and $v_{\rm micro}$= 3.20 ± 0.05 km s^{-1}. These parameters were used to calculate the synthetic spectrum.

The uncertainties of the parameters are in the range of the internal errors of the method applied. However, we should emphasize that the gravity of the star is uncertain, and as a result, the real values of effective temperature and abundances may be different from ours, which is a result

of shortcomings of the model atmosphere method applied to supergiants.

2.4 Synthetic spectrum and line identification

The final synthetic spectrum was calculated using Kurucz (1993) SYNTHE program and line data. Additional line data were taken from the DREAM database, as well as data from Morton (2000), Biemont et al. (2002), Piskunov et al. (1995), and other sources.

We estimated the projected rotational velocity of the star by iteratively matching our atlas of α Per with the synthetic spectrum, convolved with a Gaussian profile of different widths, and found that $v \sin i = 20$ km s^{-1}. Because of the problem in the determination of reliable effective temperature for the model atmosphere, no efforts were made to remove lines with uncertain oscillator strengths. Synthetic spectra serve for line identification only. An accurate analysis of chemical composition of the star is a separate task beyond our current work.

2.5 Summary

We have presented a high-resolution, and high signal-to-noise ratio atlas of α Per , together with a synthetic spectrum and line identification tables. All data can be downloaded in digital form from the Bohyunsan Observatory Web site (see footnote 2). We hope that the atlas provides

useful information for future studies as an example of a high-quality spectrum of an F5 Ib supergiant.

The synthetic spectrum is calculated within the limits of static, plane-parallel, blanketed model atmospheres that does not reach full agreement between observed data and some fundamental parameters such as gravity. However, the final synthetic spectrum adequately represents most of the spectral features of α Per and can be used for identification purposes.

References

Albayrak, B., Gulliver, A. F., Adelman, S. J., Aydin, C., & Kocer, D. 2003, A&A, 400, 1043

Alekseeva, G. A., Arkharov, A. A., Galkin, V. D., Hagen-Thorn, E. I., Nikanorova, I. N., Novikov, V. V., Novopashenny, V. B., Pakhomov, V. P., Ruban, E. V., Shchegolev, D. E. 1997, 1997 Baltic Astron., 6, 481

Andrievsky, S. M., Egorova, I. A., Korotin, S. A., & Burnage, R. 2002, A&A, 389, 519

Biemont, J., Palmeri, P., & Quinet, P. 2002, Database of rare earths at Mons University http://www.umh.ac.be/∼astro/dream.html

Castelli, F., & Hubrig, S. 2004, A&A, 425, 263

Dellbouille, L., Rolland, G., & Neven, L. 1973, Photometric Atlas of the Solar Spectrum from λ 3000 to λ 10000, (Institute de Astrophisique de Universitete de Liège).

Evans, N. R., Teays, T. J., Taylor, L. L., Lester, J. B., & Hindsley, R. B. 1996, AJ, 111, 2099

Galazutdinov, G. A. 1992, Preprint 92, SAO RAN (Spets. Astrofiz. Obs. Ross. Akad. Nauk, Nizhnij Arkhyz), 1

Galazutdinov, G. A., Musaev F. A., Krełowski, J., & Walker, G. A. H. 2000, PASP, 112, 648

Glushneva, I. N., Doroshenko, V. T., Fetisova, T. S., Khruzina, T. S., Kolotilov, E. A., Mossakovskaya, L. V., Ovchinnikov, S. L., & Voloshina, I. B. 1984, Trudy Gosud. Astron. Inst. Shternberga, 54, 3

Gopka, V. F., Yushchenko, A. V., Mishenina, T. V., Kim, C., Musaev, F. A., & Bondar, A. V. 2004, Astronomy Reports, 48, 577

Gray R. O. 1991, A&A, 252, 237

Gulliver, A. F., Adelman, S. J., & Friesen, T. P. 2004, A&A, 413, 285

Hinkle, K., Wallace, L., Valenti, J., & Harmer, D. 2000, Visible and Near Infrared Atlas of the Arcturus Spectrum 3727-9300 Å ed. Kenneth Hinkle, Lloyd Wallace, Jeff Valenti, and Dianne Harmer. (San Francisco: ASP) ISBN: 1-58381-037-4, 2000

Hirata, R., & Horaguchi, T. 1995, SIMBAD Catalog VI/69

Kharitonov, A. V., Tereshchenko, V. M., & Knyazeva, L. N. 1988, Spectrophotometric Catalogue of Stars, Alma-Ata, Nauka, 484 p.

Kunzli, M., North, P., Kurucz, R. L., & Nicolet, B. 1997, A&AS, 122, 51

Kurucz, R. L., Furenlid, I., Brault, J., & Testerman, L. 1984, National Solar Observatory Atlas, Sunspot, New Mexico: National Solar Observatory, 1984

Kurucz, R. L. 1993, CDROMs No. 1-23 (Cambridge, MA, Smithsonian Astrophys. Obs.)

Kurucz, R. L. 1995, ASP Conf. Ser. 81: Laboratory and Astronomical High Resolution Spectra, 81, 583

Morgan, W. W., & Kellman, Edith 1943, Science, 97, 536

Morton, D. C. 2000, ApJS, 130, 403

Mozurkewich, D., Armstrong, J. T., Hindsley, R. B., Quirrenbach, A., Hummel, C. A., Hutter, C. J., Johnston, K. J., Hajian, A. R., Elias II, N. M., Buscher D. F., & Simon, R. S. 2003, AJ, 126, 2502

Nordgren, T. E., Sudol, J. J., & Mozurkevich, D. 2001, AJ, 122, 2707

Piskunov, N. E., Kupka, F., Ryabchikova, T. A., Weiss, W. W., & Jeffery, C. S. 1995, A&AS, 112, 525

Shorlin, S. L. S., Wade, G. A., Donati, J.-F., Landstreet, J. D., Petit, P., Sigut, T. A. A., & Strasser, S. 2002, A&A, 392, 637

Takeda, Y., Takata-Hidai, M., 1995, PASJ, 47, 169

Takeda, Y., Takata-Hidai, M., 1998, PASJ, 50, 629

Takeda, Y., Takata-Hidai, M., 2002, PASJ, 52, 113

Tody, D. 1986, "The IRAF Data Reduction and Analysis System" in Proc. SPIE Instrumentation in Astronomy VI, ed. D. L. Crawford, 627, 733

Yushchenko, A. V. 1998, in Proceedings of the 20th Stellar Conference of the Czech and Slovak Astronomical Institutes, Ed. by J. Dusek (ISBN 80-85882-08-6, Brno), p. 201.

Yushchenko, A. V., Gopka, V. F., Khokhlova, V. L., Musaev, F. A., & Bikmaev, I. F. 1999, Astron. Lett., 25, 453

Chapter 3

Precise Radial Velocities of Polaris: Detection of Amplitude Growth

Abstract[1]

We present the first results of a long-term program of a radial velocity (RV) study of Cepheid Polaris (F7 Ib), with the aim of finding the amplitude and period of its pulsations and the nature of its secondary periodicities. A total of 264 new precise RV measurements were obtained during 2004–2007 with the fiber-fed echelle spectrograph Bohyunsan Observatory Echelle Spectrograph (BOES) of 1.8 m telescope at Bohyunsan Optical Astronomy Observatory (BOAO) in Korea. We find a pulsational RV amplitude and period of Polaris for the three seasons 2005.183, 2006.360, and 2007.349 as 2K = 2.210 ± 0.048 km s^{-1}, 2K = 2.080 ± 0.042 km s^{-1}, and 2K = 2.406 ± 0.018 km s^{-1} respectively, indicating that the pulsational amplitudes of Polaris that had decayed during the last century are now increasing rapidly. The pulsational period was also found to be increasing. This is the first detection of a historical turnaround of a pulsational amplitude change in the Cepheids. We clearly find the presence of additional RV variations on a time scale of about 119 days and an amplitude of about ± 138 m s^{-1}, which is quasi-periodic rather than strictly periodic. From our data, we do not confirm the presence of the variation on a timescale of 34–45 days found in the RV data obtained in the 1980s and 1990s. We assume that both the 119 day quasi-periodic, noncoherent variations found in our data and

[1]Chapter 3 is published in the May 2008 issue of *The Astronomical Journal*, Vol. 135: 2240-2244

the 34–45 day variations found previously can be caused by the 119 day rotation periods of Polaris and by surface inhomogeneities such as single- or multiple-spot configuration varying with time.

3.1 Introduction

Polaris (α UMi, HIP 11767, HD 8890, HR 724) is one of the most famous Cepheid variable stars. In addition to its special location on the celestial sphere, Polaris has many interesting astrophysical features. It is a member of a triple system, and it is the brightest and the closest Cepheid variable with very low pulsational amplitude. It has been extensively studied over one and a half centuries for pulsational amplitude and period changes using photometric and spectroscopic observations. Perhaps the most remarkable feature of Polaris as a Cepheid variable is that the period and amplitude of pulsation changes very rapidly. The pulsation period rapidly increases at a rate of about 4.5 s y^{-1} (Turner et al. 2005 and references herein). More interesting is the change of amplitude. It has been discovered that the pulsational amplitude has been decreasing dramatically during the 20th century (Arellano Ferro 1983; Dinshaw et al. 1989). So it was predicted that the pulsation of Polaris would completely stop by the end of the century. However, Kamper & Fernie (1998) noted that the decline in the radial velocity (RV) amplitude had stopped abruptly. Figure 5 of Hatzes & Cochran (2000) shows the

increase of amplitude, but they did not state this explicitly. Some recent photometric observations also indicate the same trend in the amplitude (Davis et al. 2002; Engle et al. 2004).

3.2 Observations and data reduction

The new RV observations of Polaris were carried out during 2004 November to 2007 June using the fiber-fed high-resolution (R = 90,000) echelle spectrograph Bohyunsan Observatory Echelle Spectrograph (BOES) (Kim et al. 2007) attached to the 1.8 m telescope at Bohyunsan Optical Astronomy Observatory (BOAO). Using a 2k x 4k CCD, the wavelength coverage of BOES is 3600–10500 Å with ∼80 spectral orders in one exposure. Observations were acquired through an iodine absorption cell (I_2) to provide the precise RV measurements. A total of N = 264 spectra were recorded; the exposure time varied from 60 to 300 s depending on the sky condition to get a typical signal-to-noise ratio (S/N) of 250. The extraction of normalized 1D spectra was carried out using the Interactive Reduction and Analysis Facility (IRAF) (Tody 1986) software package. After extracting normalized 1D spectra, the RV measurements were undertaken using a code called RVI2CELL (Han et al. 2007) which was developed at BOAO. RVI2CELL adopts basically the same algorithm and procedures described by Butler et al. (1996).

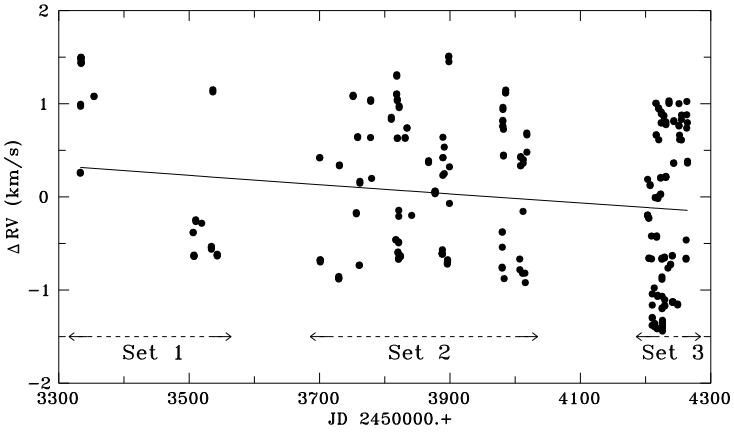

Figure 3.1: RV measurements of Polaris during 2004–2007. The solid line shows the decline of orbital RVs within the interval of observations.

However, we model the instrument profile using the matrix formula descried by Endl et al. (2000). We solved the matrix equation using singular value decomposition instead of the maximum entropy method adopted by Endl et al. (2000). With these configuration, we achieved a typical internal RV accuracy between 10 and 15 m s^{-1} depending on the quality of the spectra.

3.3 Results

Figure 3.1 plots the relative RV measurements for the 2004–2007 season of observations. The solid line is a zero-point-adjusted trend for a binary orbit calculated according to the period of 29.59 years and orbital elements given by Wielen et al. (2000). To study pulsations, we first removed the RV variation due to orbital motion. Next, we applied the discrete Fourier Transform (DFT) analysis for unequally spaced data to all de-trended 2004–2007 RV data. We used for analysis the computer code PERIOD04 (Lenz & Breger 2005). The top panel in Figure 3.2 shows the resulting DFT periodogram of all data. We easily found a main frequency of $f_1 = 0.251757 \pm 0.000008$ c d^{-1} ($P_1 = 3.97208 \pm 0.00013$ days). The whole 2004–2007 data phase diagram of Polaris phased with this period is plotted in Figure 3.3. There are visible scatters, and two order values (near JD 2453902) exceed the accuracy of our individual RV measurements ($\sim$10 m s^{-1}).

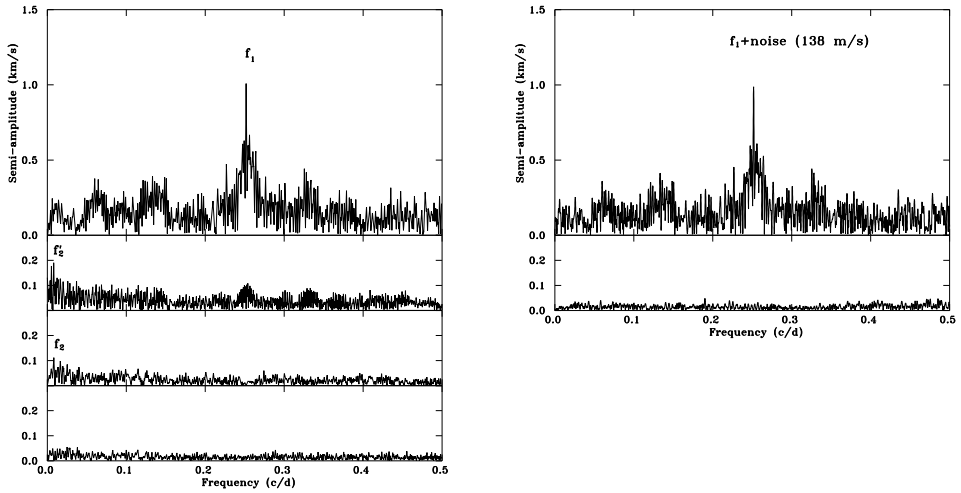

Figure 3.2: The amplitude spectra of DFT analysis for the entire RV measurements for Polaris. Left panel: (top) DFT of the original data. The largest peak is at $f_1 = 0.251757$ c d^{-1}. (Second) DFT of RV residuals after removal of the contribution from f_1. The second peak is at $f_2{}' = 0.00799$ c d^{-1}. (Third) DFT of the merged residual RV after removal of the best-fit f_1 contribution from individual subsets (Sets 1–3). The secondary peak is at $f_2 = 0.00840$ c d^{-1}. (Bottom) DFT of the residuals after removal of f_1 and f_2. Right panel: (top) the amplitude spectrum of an artificial sin-wave signal having the same frequency, amplitude, and data point sampling as the dominant f_1 mode but co-added with normally distributed noise of the the amplitude of 138 m s^{-1}. (Bottom) DFT of the residual RV after removal of the contribution from f_1.

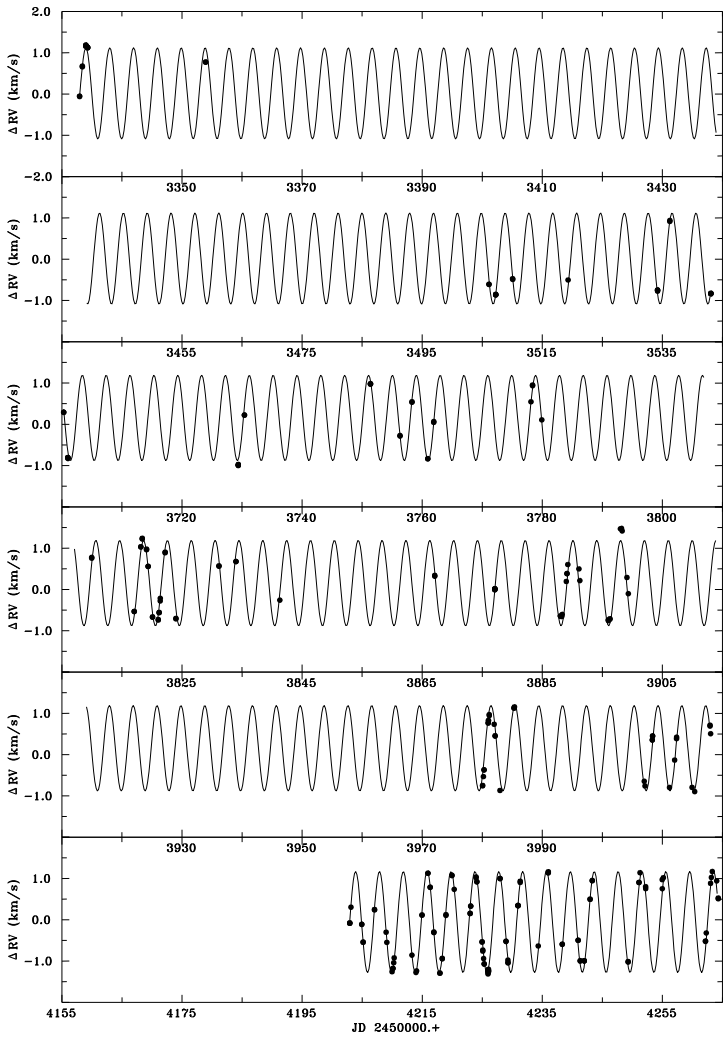

Figure 3.3: Entire RVs of Polaris de-trended for orbital variations. The solid line is a dominant period fit to every subsets of the data.

Table 3.1: The period and amplitude of Polaris

Data	Mean epoch (duration)	N	σ (km s^{-1})	Semi-amplitude (km s^{-1})	Dominant Period (days)	Period in res. (days)
Dinshaw	1987.674 (0.660)	174	0.661	0.742 ± 0.068	3.97206 ± 0.00307	45
Hatzes	1992.693 (1.698)	40	0.140	0.755 ± 0.032	3.97212 ± 0.00056	17, 40
Kamper1	1994.492 (0.414)	71	0.098	0.786 ± 0.017	3.97208 ± 0.00081	34
Kamper2	1995.973 (1.249)	129	1.107	0.825 ± 0.013	3.97200 ± 0.00029	
set 1	2005.183 (0.575)	34	0.111	1.105 ± 0.024	3.97300 ± 0.00080	\
set 2	2006.360 (0.870)	117	0.149	1.040 ± 0.021	3.97284 ± 0.00047	⟩ 119
set 3	2007.349 (0.168)	113	0.063	1.203 ± 0.009	3.97394 ± 0.00098	/

This scatter seems to be due to additional intrinsic RV variations to the dominant pulsation mode, already known for Polaris (Dinshaw et al. 1989; Kamper 1996; Kamper & Fernie 1998; Hatzes & Cochran 2000). We removed the best-fit sine-wave signal from the dominant period from the whole data string. The DFT analysis of RV residuals is shown in second from top panel in Figure 3.2. The highest peak at $f_2^{'} = 0.00799$ $\pm$ 0.00010 c d^{-1} ($P_2{}^{'} = 125.1 \pm 0.1$ days) has an amplitude of 2K = 0.38 $\pm$ 0.02 km s^{-1}.

One might suspect that the secondary signal at $f_2^{'}$ found in our 2004–2007 data residuals is due to the removal of dominant pulsations with fixed amplitude and period which actually vary during this time interval. Here, our main concern is to estimate the amplitude and period of the dominant pulsations for short subsets as accurately as possible and remove them from RV variations in order to study possible residual signals. In determining the period and amplitude variation, the data were divided into three subsets: Set 1, Set 2, and Set 3. These subsets are marked in Figure 3.1. The RV data characteristics are given in second, third, and forth columns of Table 3.1. Then, for each data set, we tried to find best-fit frequency and amplitude for a dominant pulsation. Figure 3.4 shows a dominant period fit to every subset of the data. The rms residuals after the sinusoidal fitting of Sets 1–3 are 111 m s^{-1}, 149 m s^{-1}, and 63 m s^{-1} respectively, much larger than the typical error of RV data, 10–15 m s^{-1}.

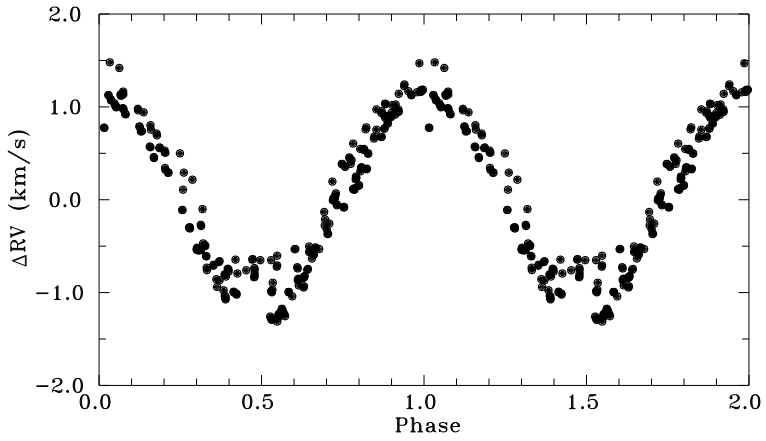

Figure 3.4: Phase curve of the original data phased to the best-fit period $P_1 = 3.97208$ days.

This is because there exists unmodelled RV variation in addition to the sinusoidal signal. Table 3.1 shows the result of the period analysis: periods and amplitudes of pulsations found for all three sets. We applied the same period analysis to the most recent RV data published for Polaris. The period and amplitude found during our re-analysis are also given in Table 3.1.

To study additional variability, the residuals after removal of the best-fit dominant period and amplitude from each set were combined, resulting in the data string shown in Figure 3.5. As seen by eye, there is still very strong $\sim \pm$ 350 m s^{-1} and about 120 days timescale variability. A steep rise of RV from negative to positive values and a rapid drop back to negative values can be seen in the shape of RV variability. This type of variability resembles closely the RV variations due to a contrast surface spot passing across the visible disk in some types (e.g., Ap) of stars. To get the accurate period, the DFT analysis was applied to the residual data. The DFT amplitude spectrum is shown in the third panel from the top panel in Figure 3.2. The largest 138 $\pm$ 8 m s^{-1} peak is at f_2 = 0.00840 $\pm$ 0.00003 c d^{-1} (P_2 = 119.1 days). The residual data phased to this period shown in Figure 3.6. The DFT of residuals after removing the secondary periodicity is shown in the bottom panel in Figure 3.2; it does not show any significant peaks.

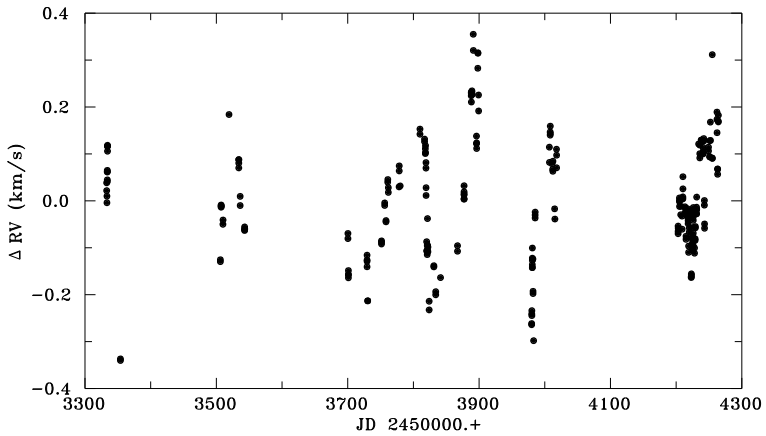

Figure 3.5: Merged residual RVs after removal of the best-fit amplitude and period solutions to the data from the three subsets.

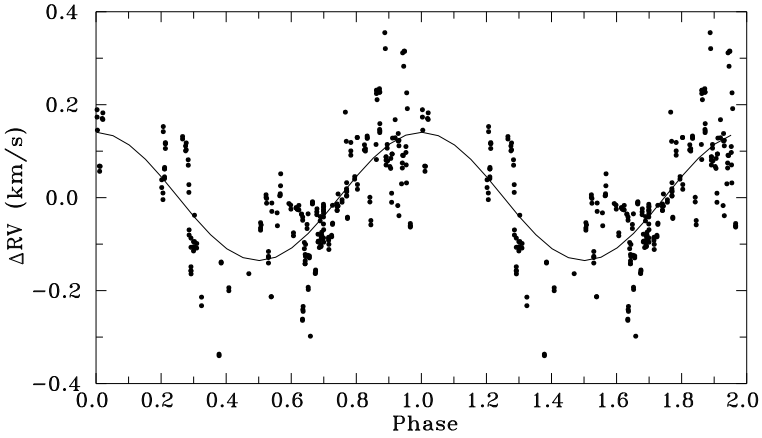

Figure 3.6: Residual RV phased with a best-fit period of $P_2 = 119.1$ day from the three subsets.

The check whether secondary periodicity may be due to unrecognized aliasing problem and unfavorable time sampling of RV data (note that the strongest sidelobes of the spectral spectral window function are 1 c d^{-1} equally spaced), we modeled the dominant mode pulsations by mono-periodic sinusoidal signal having the same time sampling as the original Polaris RV data. Note that the DFT of this mono-periodic signal is actually the spectral window function centered at f_1. We added to this mono-periodic signal the normally distributed noise with an amplitude of 138 m s^{-1}. The DFT analysis of these artificial data is shown in right panels (top and bottom) in Figure 3.6. As can be seen from the bottom panel, after removal of the artificial signal, the amplitude spectrum do not show any significant signal at 0.008 c d^{-1}, confirming that secondary 119 day periodicity we found is not an artifact.

Figure 3.7 shows a century-long variations of the pulsational amplitude and period of Polaris. As seen, our new data obtained for three subsets of our 2004–2007 observations reveals that, after a decade of standstill, the amplitude of pulsation now rapidly increase. We can now safely claim that the era of amplitude decrease of Polaris finished at the end of 1980s and was replaced with a new, rapidly rising amplitude trend at the beginning of the 1990s.

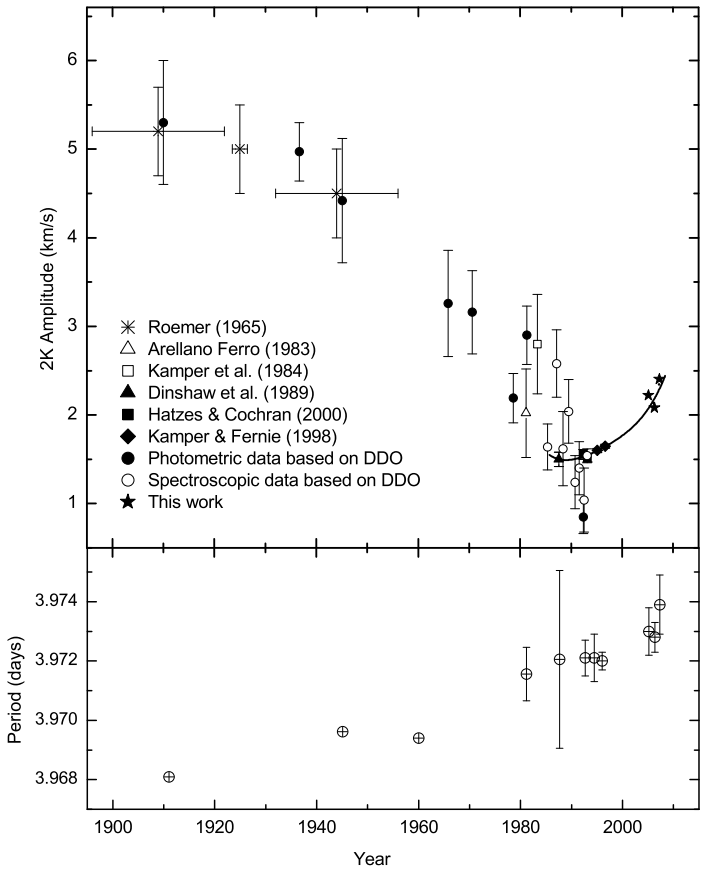

Figure 3.7: Variations of the pulsational RV amplitude and period of Polaris during the last century. (Top) Filled and open circles denote the result from DDO photometric and spectroscopic measurements, respectively. To convert photometric determination to RV determination, a conversion factor of ∼50 (Kamper & Fernie 1998, and Fernie et al. 1993) was used. The solid line is a polynomial fit to the recent RV measurements. Error bars of Hatzes & Cochran (2000), Kamper & Fernie (1998), and this work are smaller than the symbols. (Bottom) The period variations; for the first three points, there are no references for the error bars.

3.4 Discussions

A historic change of the sign of amplitude variations in Polaris, which we detected convincingly, does not yet have an analogy among other Cepheids. Polaris crosses the instability strip for the first time and lies well in its center for fundamental mode pulsators or well inside and near the hot bounds of the instability strip for first overtone pulsators (Turner et al. 2005). We suggest that the switching of the amplitude change from decay to growth found in our observation is not a direct result of evolution to a red border and the decrease of the efficiency of the excitation mechanism, but might be relevant to the unrecognized effect of mode interaction. We also confirm the increase of the pulsational period.

The detected long-term characteristic period of 119 days is much longer compared to the 9.75 days period of Kamper et al. (1984), 45.3 days of Dinshaw et al. (1989), 34.3 days of Kamper & Fernie (1998), or 40.2 days of Hatzes & Cochran (2000) reported in the 1980s and 1990s data. We do not confirm the existence of any of the aforementioned periods in our data. Dinshaw et al. (1989) argue that an approximately 45 day period, which is not coherent, arises from one or more surface features on Polaris carried across the disk by rotation. Hatzes & Cochran (2000) have found very reliable bisector variations with the same period as in the RVs and re-discussed three mechanisms of the low-amplitude

residual RV variations in Polaris: a low-mass companion, long-periodic nonradial stellar pulsations, or rotational modulation by surface features. They modeled the residual RV and bisector variations for all hypotheses – namely, the existence of a surface microturbulence, cool or hot spots and 45 day rotation period, or the $l = 4$, $m = 4$ nonradial mode pulsations and found a reliable RV amplitude fit for all of them. However, the bisector span velocity for all hypotheses had unmodeled phase shifts, indicating that none of these models completely satisfies the observations. Hatzes & Cochran (2000) concluded that among the hypotheses considered, the nonradial pulsations have better agreement with modeling.

In our work based on long-term high-precision RVs, we do not confirm any of the secondary period found earlier, but clearly a find 119.1 day characteristic time of variation. This is the longest period of intrinsic variations of Polaris found so far.

Summarizing all previous investigations, we can claim that the secondary variations seen in Polaris are not coherent on long timescales, so we can firmly reject the first two hypotheses involving the companion and coherent non-radial pulsations. Note that a period of 119 days is too long compared to a period of fundamental mode pulsations of Polaris and cannot belong to normal acoustic modes.

We suggest two possible explanations of secondary RV variations.

1) The diversity in secondary periods found in Polaris is likely the result from the rotational modulation of RVs by a single- or multiple-

surface spots and assume that the rotation period is about 119 days. In the case of multiple spots, the observed periods of about 40 days or about 34 days are close to fractions of a 119 day period. The rotational velocity of Polaris is v sin i = 8.4 km s^{-1} (Hatzes & Cochran, 2000). The radius of Polaris 33 $\pm$ 2 $R_{\odot}$ was found by Turner et al. (2005) from the distance to Polaris 94 $\pm$ 4 pc and the angular diameter 3.28 $\pm$ 0.02 mas given by Nordgren et al. (2000). With these parameters and an assumed rotation period of 119 days, the equatorial rotation velocity is $v_{\rm eq}$ = 14 km s^{-1} which yields the inclination angle of the rotation axis $i = 38°$. The projected rotational and expected equatorial velocities of Polaris are in quit good agreement with the determined mean-projected rotational velocities $\overline{vsini}$ = 15.8 $\pm$ 1.4 km s^{-1} of a sample of 11 F6-F7 Ib supergiants selected from the Ib supergiant list of De Medeiros et al. (2002).

2) We also cannot exclude that long-term cyclic variations of radial velocities of Polaris are the result of oscillatory variations of the mean radius of Polaris stochastically driven with a yet unrecognized physical mechanism. It is not excluded that such long-term, non-coherent and small radius variations are intrinsic to many F type supergiant stars and Cepheids, but in classical Cepheids they are hidden in a large amplitude of the dominant mode pulsations and have not been detected due to limited RV accuracy and sparse time sampling of RV curves in previous RV investigations. If this is true, Polaris might be the first Cepheid

star with well-documented observational detection of such a modulation. Another good example might be the F5 Ib supergiant α Per which shows long-term (see Figure 1 in Hatzes and Cochran 1995) variations. The detailed comparative precise RV study of a sample of F-type supergiant stars including Cepheids can provide additional constrains on the nature of the long-term radius variations detected in Polaris.

Checking of the spot hypothesis and detailed analysis of line profile and surface temperature variations in Polaris-based BOES observations is beyond the scope of the current work, which is devoted to the study of pulsational amplitude of RVs, and will be presented in our next paper.

3.5 Conclusions

The first results of our long-term monitoring of Polaris show remarkable changes in the amplitude and the period of pulsations that occurred at the end of 20th and the beginning of 21st century. The half-century-long pulsational amplitude decay was replaced with a rapid amplitude growth while the growth of the pulsational period continues. We also detected a 119 day secondary RV variation which is about three times longer than previously reported secondary periodicities. We concluded that 119 day variations are not coherent on long timescales and have discussed the possible nature of these variations.

References

Arellano Ferro, A. 1983, ApJ, 274, 755

Butler, R. P., Marcy, G. W., Williams, E., McCarthy, C., Dosanjh, P., & Vogt, S. S. 1996, PASP, 108, 500

Davis, J. J., Tracey, J. C., Engle, S. G., & Guinan, E. F. 2002, BAAS, 34, 1296

De Medeiros, J. R., Udry, S. Burki, G. & Mayor, M. 2002,A&A, 395, 97

Dinshaw, N., Matthews, J. M., Walker, G. A. H., & Hill, G.M. 1989, A&A, 98, 2249

Endl, M., Kürster, M., & Els, S. 2000, A&A, 362, 585

Engle, S. C., Guinan, E. F., & Koch, R. H. 2004, BAAS, 36, 744

Fernie, J. D., Kamper, K. W., & Seager, S. 1993, ApJ, 416, 820

Han, I., Kim, K.-M., & Lee B.-C. 2007, PKAS, 22, 75

Hatzes, A. P., & Cochran, W. D. 1995, ApJ, 452, 401

Hatzes, A. P., & Cochran, W. D. 2000, AJ, 120, 979

Kamper, K. W., Evans, N. R., & Lyons, R. W. 1984, JRASC, 78, 173

Kamper, K. W. 1996, JRASC, 90, 140

Kamper, K. W., & Fernie, J. D. 1998, AJ, 116, 936

Kim, K. M., Han, I., Valyavin, G. G., Plachinda, S., Jang, J. G., Jang, B.-H., Seong, H. C., Lee, B.-C., Kang, D.-I., Park, B.-G, Yoon, T. S., Vogt, S. S., 2007, PASP, 119, 1052

Lenz, P., Breger M. 2005, Commun. Asteroseismology, 146, 53

Nordgren, T. E., Armstrong, J. T., German, M.E., Hindsley R. B., Hajian, A. R., Sudol, J. J. & Hummel, C. A. 2000, ApJ, 543, 972

Roemer, E. 1965, ApJ, 141, 1415

Tody, D. 1986, Proc., 627, 733

Turner, D. G., Savoy, J., Derrah, J., Abdel-Sabour Abdel-Latif, M., & Berdnikov, L.N. 2005, PASP, 117, 207

Wielen, R., Jahreiß, H., Dettbarn, C., Lenhardt, H., & Schwan, H. 2000, A&A, 360, 399

Chapter 4

Discovery of a 395-day Radial Velocity Variations in Oscillating K-giant α Arietis – Planet or Surface Features?

Abstract

We report the detection of a low-amplitude 394.7-day radial velocity variations in the K2 III star α Arietis (HD 12929). This star belongs to our sample of 55 K-giants studied for exoplanet and pulsation searches using the fiber-fed Bohyunsan Observatory Echelle Spectrograph (BOES) attached to the 1.8-m telescope at Bohyunsan Optical Astronomy Observatory (BOAO) in Korea. Precise radial velocity (RV) measurements of α Arietis were obtained during November 2003 to October 2008. We do not found the correlation between RV variations and equivalent widths of chromospheric activity indicators (Hα and CaII 8662Å line). The bisector analysis, indeed shows that bisector velocity span (BVS) and RV variations are strongly correlated with each other, while we do not find the 395-day period in variations in BVS. We concluded that the RV variations are produced, in major, by intrinsic changes of shapes of spectral lines due to the surface spots. We cannot indeed safely reject the exoplanet hypothesis as a reason of at least part of RV variations. We find a possible orbital solution for RV variations with a period of $P = 395$ days, a semi-amplitude of $K = 65$ m s^{-1}, and an eccentricity of $e = 0.25$. Assuming a possible stellar mass of $M_\star = 1.4$–5.6 $M_\odot$, we estimate a minimum mass for the companion of $m_2 \sin i = 2.8$–7.2 M_{Jup} with an orbital semi-major axis of 1.2–1.9 AU. α Ari becomes the most massive star that has a planetary companion. And, our discovery gives

a support to search for exoplanets around giant star with multi-periodic oscillations.

4.1 Introduction

Since the first extra-solar planet around a main sequence star was discovered by Mayor & Queloz (1995), more than 450 extra-solar planets have been found so far. Most of them are found around main sequence stars using the precise radial velocity (RV) method, but several planets have been found around giant-type stars. Frink et al. (2002) discovered the first extra-solar planet around the K-giant star ι Dra (K2III). Thereafter, several companions around K giant stars have been reported using the precise RV method (Setiawan et al. 2003a, 2003b, Mitchell et al. 2003, Hatzes et al. 2005, 2006, Reffert et al. 2006, Johnson et al. 2007, 2008, Döllinger et al. 2007, Sato et al. 2007, 2008). Nowadays, it is known that the velocity variations caused by planetary companions in giant star are blended with the stellar pulsations and surface activities.

K giant α Ari (HD 12929) is one of our sample 55 K giant stars of which we have obtained precise RV measurements for the past five years. In previous publication, we (Kim et al. 2006) reported about multi-periodic oscillations in α Ari with periods $P_1 = 0.571$ day (or aliases at 0.445 or 0.871 days) observed during November to December 2003. The average amplitude variation cover $\sim \pm$ 20 m s $^{-1}$ just overnight. The

variability can only be the result of stellar oscillations because of the short time scale. We continued to observe α Ari getting several spectra in every night to search for long-term variation. Here we report on discovery a long-period RV variation of α Ari.

4.2 The properties of α Ari

We refer main photometric parameters of Allende Prieto & Lambert (1999) taken from the Hipparcos catalogues of stars within 100 pc from the Sun and refer main spectroscopic parameters of Hekker and Meléndez (2007) taken at Lick observatory.

The mean RV of α Ari is – 14.2 km s^{-1} (Evans, 1967). Gray et al. (2002) determined $T_{\rm eff}$ = 4481 ± 11 K and [Fe/H] = – 0.221 ± 0.036. Mozurkewich et al. (1991) measured an angular diameter for α Ari of 6.412 ± 0.064 mas at 800 nm. The Hipparcos parallax of 49.48 ± 0.99 mas results in a stellar radius of 13.9 ± 0.3 $R_{\odot}$.

The most recent determinations of the projected rotational velocity v_{rot} sin i = 3.44 km s^{-1} by Hekker and Meléndez (2007) and 3.1± 1 km s^{-1} by Carney et al. (2008) are close to each other. Based on the last value that is given with error estimation, we derived the range of upper limit of the rotational period of

$P_{rot} = 2\pi$R / (v_{rot} sin i) = 172–335 days.

Table 4.1: Stellar parameters for α Ari.

Parameter	Value	Unit
Spectral type	K2III	
m_v	2.01	[mag]
M_v	0.48 ± 0.09	[mag]
B-V	1.151	[mag]
Parallax	49.48 ± 0.99	[mas]
Angular diameter	6.412 ± 0.064	[mas]
Distance	20.2	[pc]
RV	– 14.6 ± 0.1	[km s^{-1}]
$T_{\rm eff}$	4481 ± 11	[K]
[Fe/H]	– 0.221 ± 0.036	[dex]
log g	2.6 ± 0.3	
$M_\star$	1.4–5.6	[$M_\odot$]
$R_\star$	13.9 ± 0.3	[$R_\odot$]
v_{rot} sin i	3.44 or 3.1±1	[km s^{-1}]
P_{rot} / sin i	172–335	[days]
v_{micro}	1.7	[km s^{-1}]
v_{macro}	2.66	[km s^{-1}]

Berdyugina et al. (1991) determined log g = 2.6 $\pm$ 0.3 from the result of testing the compatibility of atmospheric analysis giants at the Crimean Astrophysical Observatory and the Main Astronomical Observatory. Surface gravity and its uncertainly log g = 2.6 $\pm$ 0.3 yields a stellar mass in the range of 1.4 – 5.6 $M_{\odot}$. The basic stellar parameters of α Ari are listed in Table 4.1.

4.3 Observations and analysis

The spectra of α Ari were acquired during November 2003 to October 2008 using the fiber-fed high resolution (R = 90 000 at 5000 Å) echelle spectrograph BOES (Kim et al. 2007) attached to the 1.8-m telescope at BOAO in Korea. Iodine absorption cell (I_2) was used to provide the precise RV measurements. Each estimated S/N ratio at I_2 wavelength region is about 250 with typical exposure time ranging between 90 and 180 seconds.

The extraction of normalized 1–D spectra was carried out using IRAF (Tody 1986) software. Further data processing, I_2 analysis and precise measurements were undertaken using a code called RVI2CELL (Han et al. 2007) developed in Korea Astronomy & Space Science Institute (KASI). Also, to demonstrate a long-term stability of the BOES we show a standard star τ Ceti in Figure 4.1. It shows that τ Ceti is constant with rms scatter of 7.5 m s^{-1}, over a time span of 5 years during our program.

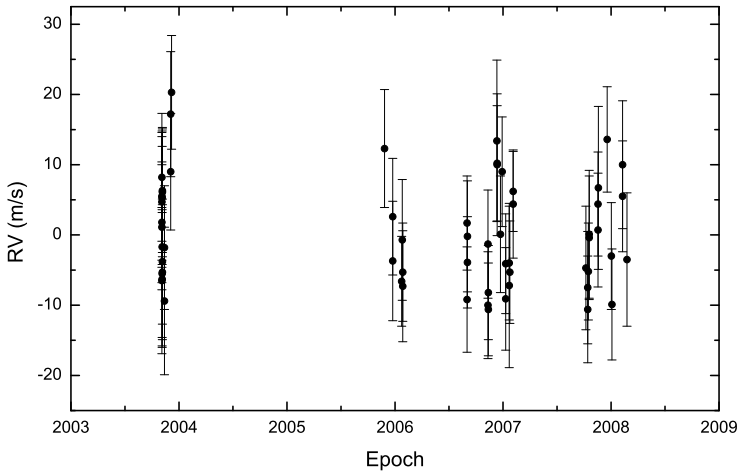

Figure 4.1: RV measurements of a standard star τ Ceti during 2003 and 2008.

4.4 Orbital solution

The long-term variation of α Ari was first noted by Walker et al. (1989) and Larson et al. (1999) who used CFHT 3.6-m and DAO 1.8m telescopes with hydrogen-fluoride (HF) absorption cell. These data were insufficient (45 spectra) to draw any conclusions about possible periodic variability. We recalculated the standard deviation of their 45 measurements of RV variation of $\sigma_{\rm CFHT} = 41.6 \pm 6.2$ m s^{-1} during 13 years. This is consistent with the ($\sigma_{\rm BOAO} = 42.7 \pm 1.9$ m s^{-1}) of whole BOAO data. The individual RV measurements are shown on the top panel in Figure 4.2 (dots), they exhibits clear variations with period about four hundred days.

We found the period of variations is $P = 394.7 \pm 0.3$ days and semi-amplitude is K = 65.0 ± 0.9 m s^{-1}. The solid line in the top panel of Figure 4.2 is the best fit Keplerian orbit. The eccentricity of orbit is e = 0.25 ± 0.02. We estimate the minimum mass of the companion to be 2.8–7.2 M_{Jup} with orbital radius of 1.2–1.9 AU.

The rms residual from the orbital solution is 18.4 m s^{-1} (Figure 4.2). This almost certainly is due to the short period variations and intrinsic variability of stellar oscillations, as shown by Kim et al. (2006). All the orbital elements are listed in Table 4.2. RV-phase diagram for the orbit in Figure 4.2 is shown in Figure 4.3. It shows that the long-period with the low-amplitude variation is more apparent.

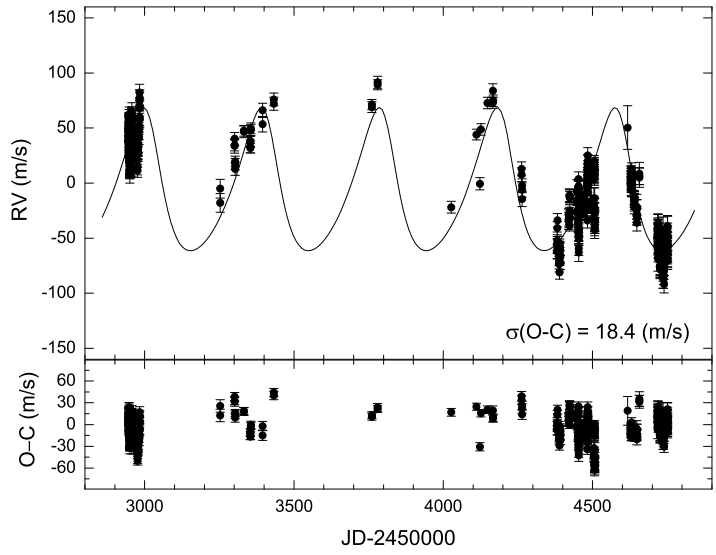

Figure 4.2: RV measurements (Top) and rms scatter of the residuals (Bottom) for α Ari taken at BOAO from November 2003 to October 2008. The solid line is the orbital solution with a period of 394.7 days and an eccentricity of 0.25.

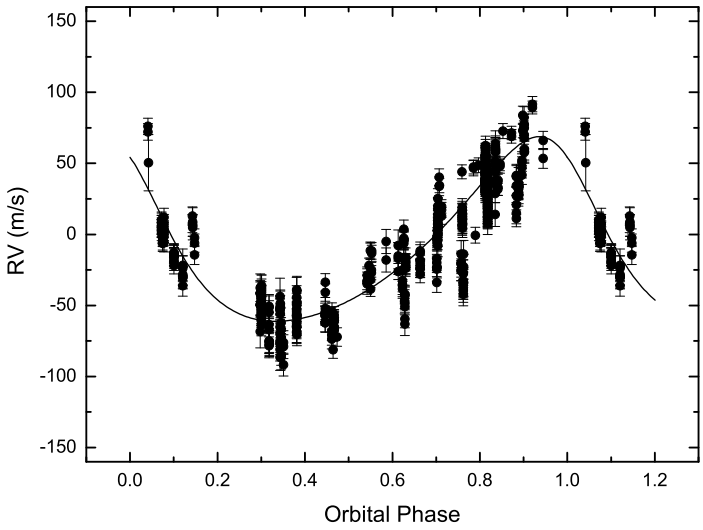

Figure 4.3: RVs of α Ari phased to the period 394.7 days. The solid line is the orbital solution that fits the data with rms of 18.4 m s $^{-1}$.

Table 4.2: Orbital parameters of the RV measurements for α Ari b.

Parameter	Value	Unit
Period	394.7 ± 0.3	[days]
$T_{\text{periastron}}$	2451443.44 ± 2.01	[JD]
K	65.0 ± 0.9	[m s^{-1}]
e	0.25 ± 0.02	
ω	38.96 ± 1.78	[deg]
$f(m)$	(1.0174) × 10^{-8}	[$M_{\odot}$]
$m \sin i$	2.8–7.2	[M_{Jup}]
a	1.2–1.9	[AU]
σ (O-C)	18.4	[m s^{-1}]

4.5 The nature of the RV variations

α Ari is a K-giant star. These stars exhibits pulsational as well as surface activity resulted in low-amplitude RV variability at different time scales. To establish whether the low-amplitude and long-term RV variations are caused by surface activity we examined the stellar chromospheric activity indicators like the equivalent width of sensitive lines and spectral line bisectors. The Hipparcos photometry was also examined.

4.5.1 Hipparcos photometry

We analyzed the Hipparcos photometry for α Ari in order to search for possible brightness variations due to the surface spots. For 2.5 years Hipparcos satellite obtained 66 photometric measurements of α Ari, and we used the whole data except one measurement with a large error. Figure 4.4 shows the periodogram of Hipparcos photometric measurement near the orbital frequency of α Ari (the vertical dot line). There is no significant peaks near the frequency corresponding to 395 day period (0.0025 c/d) as well in whole frequency interval 0–0.03 c/d.

4.5.2 Chromospheric activity indicators

The equivalent widths (EW) of Ca II H & K, H_α, Ca II 6882 $\mathring{A}$, and He I 1 0830 $\mathring{A}$ are frequently used for chromospheric activity analysis.

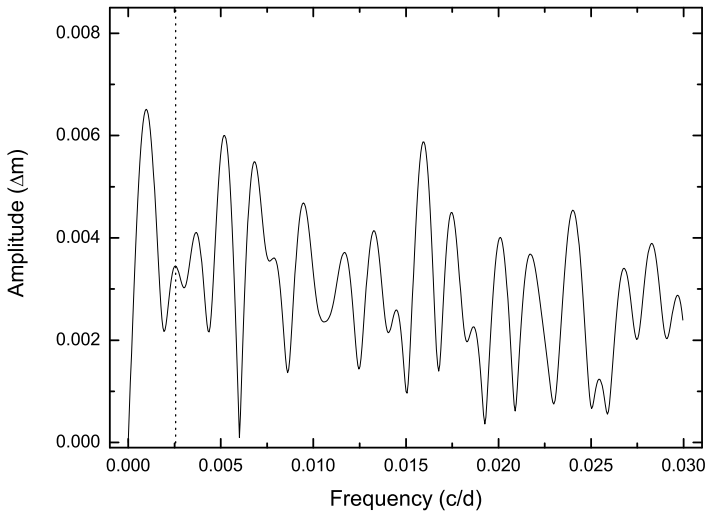

Figure 4.4: Periodogram of the Hipparcos photometry for 2.5 years. The vertical dot line marks the location of the orbital frequency.

The Balmer H_α can be useful for discerning where RV variation is due to intrinsic stellar variability (Kürster et al. 2003). Unlike main sequence stars, where H_α is blended with telluric and broad lines, giant star is much easier to measure the EW of H_α. The mean EW of the H_α in α Ari is measured to be 1086.7 $\pm$ 10.7 mÅ. The rms of 10.7 mÅ corresponds to 0.98 % variation in the EW.

Figure 4.5 (top panel) show the H_α line EW variations with time. No any significant variability was found vs JD. To find any relationship of variations in the EW of the H_α and the RV we plot two parameters EW and RV in Figure 4.6. The low value of correlation coefficient K=0.22 (Press et al. 2007) revealed that EWs are not strongly correlated with RV variations. We conclude that the rotational modulation is not present or has too small amplitude to be resolved in H_α-line EW variation data.

Figure 4.5 (bottom panel) show the Ca II 8662 $\mathring{A}$ line EW variations with time. Again, no any significant variability with period of 395 day was found. Figure 4.7 shows the diagram of Ca II 8662 $\mathring{A}$ line EWs vs measured RVs. The low correlation coefficient K=0.2612 show that these data are not strongly correlated. Thus, we found no evidences of strong correlation between EWs of H_α and Ca II 8662 $\mathring{A}$ lines with the RV.

Another two activity indicators are unqualified; Ca II H& K lines do not have enough S/N ratios to estimate EW variations reliably and He I 1 0830 $\mathring{A}$ is out of the range in our data.

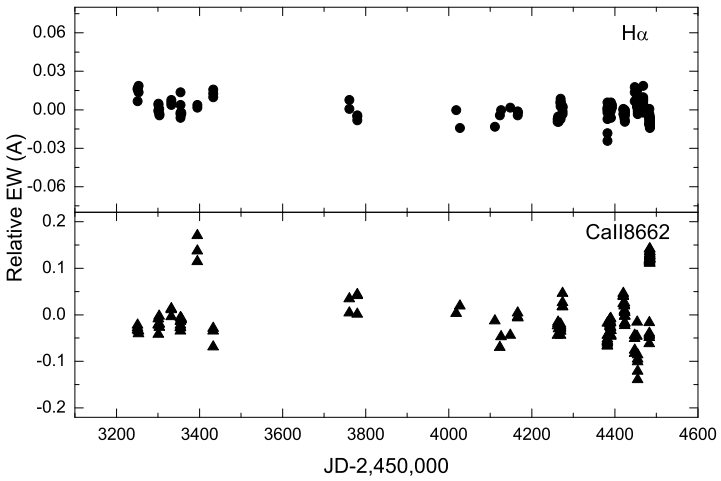

Figure 4.5: EWs vs JD of H_α and Ca II 8662Åfor α Ari in interval between September 2004 and October 2008.

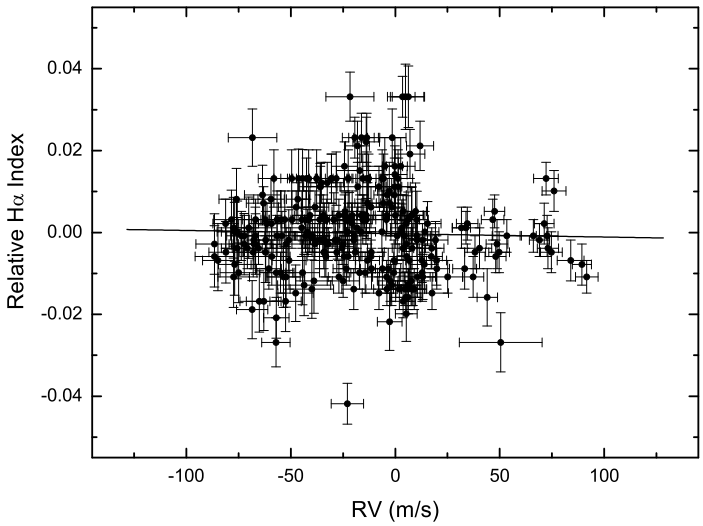

Figure 4.6: EWs vs RVs of the H_α. The diagram shows no correlation between the EWs and the RVs.

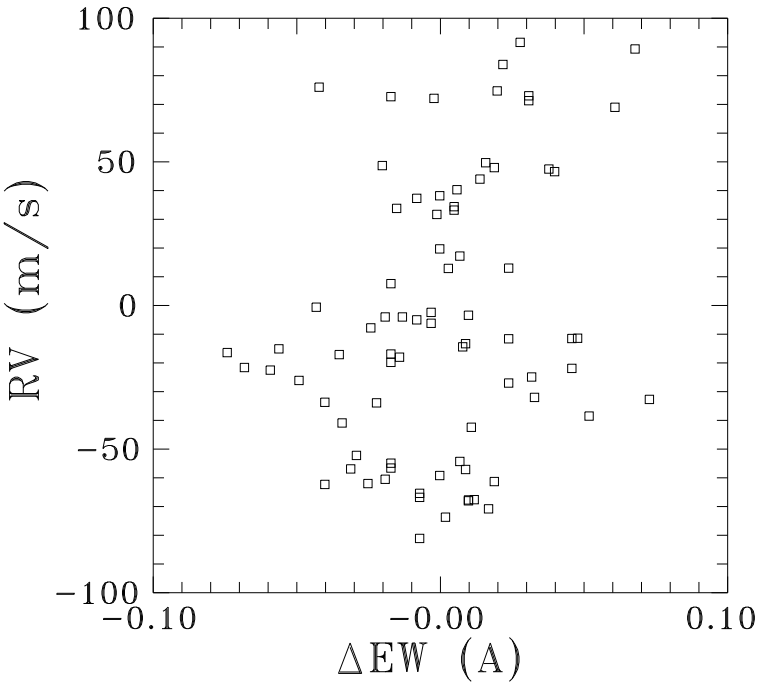

Figure 4.7: The Ca II 8662 $\mathring{A}$ EW vs RVs.

4.5.3 Line bisector variations

Queloz et al. (2001) reported that the analysis of the line bisector can distinguish the origin of the observed RV variations. It is very useful for the messy star, such as K-giant, that can have several kinds of RV variations blended with pulsations, surface spots and planetary companions. The RV variations due to planetary companions should not produce change in the spectral line shape, while the surface inhomogeneities do. Surface features and stellar rotation modulation can create variable asymmetries in the spectral line profiles. Thus, the analysis of the shapes of spectral lines could prove or disprove the existence of planetary companions.

We calculated the mean profile of spectral lines using the least squares deconvolution (LSD) technique (Reiners & Royer 2004). We used the Vienna Atomic Line Database (VALD; Piskunov et al. 1995) to prepare the list of spectral lines. The total 4339 lines within wavelength region of 4500 – 4900 and 6450 – 6840 Å were used for the construction of the LSD profile, which are excluded spectral regions around I_2 absorption region, hydrogen lines and regions with strong contamination by terrestrial atmospheric lines. We measured the bisector velocity span (BVS) of a mean profile between central depth levels 0.8 and 0.25 as the span points.

The variations of BVS vs JD are shown in Figure 8. As seen, the BVS in the interval 2454453-2454506 (shown by open circles) are shifted in

respect on preceding and following data on amount of above +160 m s^{-1}. We found that this bias is due to temporary mis-alignments of the BOES echelle spectrometer, that was later (since JD 2454617) corrected. While the RV code RVI2CELL takes into account any changes of instrumental profile in calculations of RVs, this misalignment does not affected the RV data.

To increase of sensitivity in searching possible BVS and RVs correlations and to excluded effect of long-term instrumental profile instabilities of the BOES we selected for analysis three short time intervals JD 2453301-2453432 (data set I), JD 2454027-2454393 (II), JD 2454617-2454751 (III) that corresponds the high rates of RV changes (ascending and descending branches of RV curves). We assumed that the BVS data in these short time intervals do not affected by long-term variations of instrumental profile that can mimic the short-term intrinsic variations.

Figure 4.9 shows the BVS vs the RV variations plotted by filled circles, open circles and crests for intervals I, II and III respectively. The dashed lines shows the linear fit to the data. As seen, the BVS variations from these intervals are linearly dependent from the RV variations BVS= B_i·RV + A_i, with coefficients B_i= 0.597; 0.524; 0.540 and A_i= –370; –340; –268 for intervals I, II and III respectively and are strongly correlated.

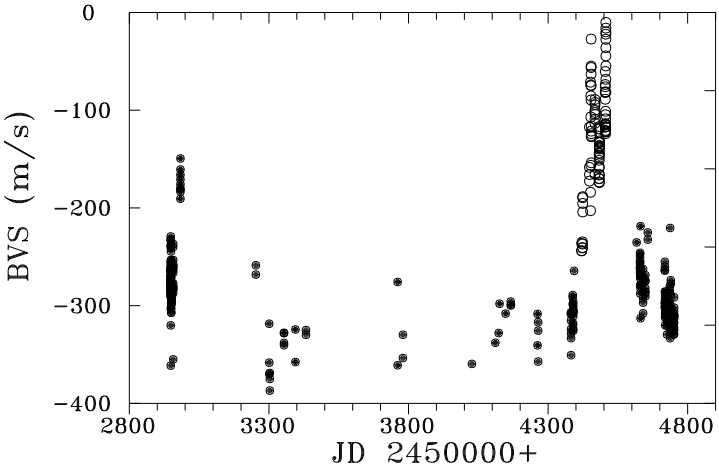

Figure 4.8: BVS variations between November 2003 to October 2008. The data affected by strong instrumental BVS shifts are shown by open circles (see text).

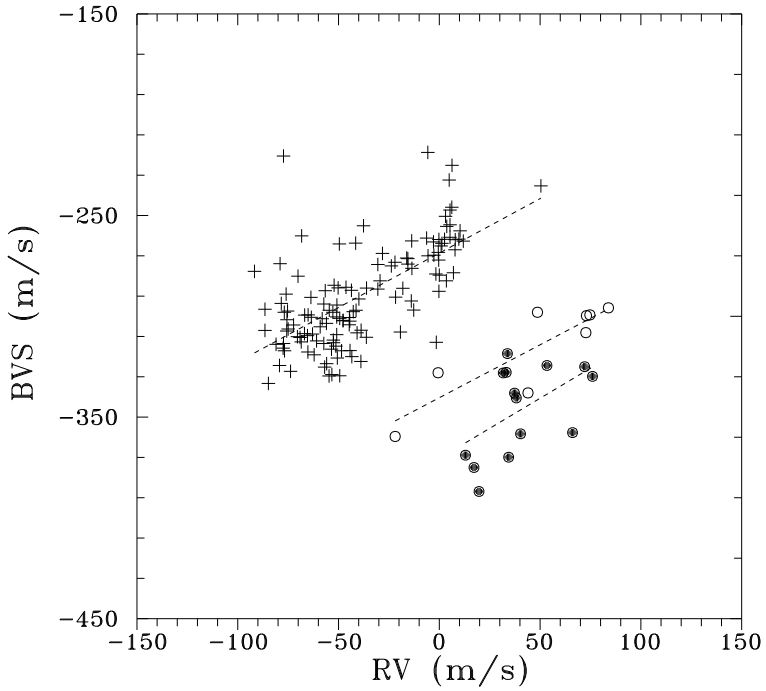

Figure 4.9: BVS vs RV variations for selected data intervals that corresponds to fast RV changes (see text).

The correlation coefficient (K) and probabilities (P) that the data are not correlated are K_i=0.521, 0.864, 0.657 and P_i=3.6 10^{-2}, 5.2 10^{-4}, 9.1 10^{-19} for sets I, II and III respectively. The BVS zero point instrumental shift of about 87 m s^{-1} between intervals I, II and III is indeed present between these data spread over interval of 1450 days. These results clearly shows that observed RV variations in α Ari are induced with intrinsic line profile variations most probably caused by by surface spots and the rotation of a star.

4.6 Discussion and conclusion

Our analysis of the RV measurements for α Ari shows that the existence of a long-period and a low-amplitude variation. Stellar oscillations in α Ari have much shorter time scale (Kim et al. 2006) and can be excluded as a reason of long-term variations. We do not found any variations in EWs of Hα and Ca II 8662 $\AA$ line as well as in Hiparcos photometry.

However, we found strong evidences that RV correlated with line bisector variations and can be caused by rotational modulations by surface features.

Our estimate of the rotation period for α Ari is 172–335 days, that is shorter than period of 394.7 days found in the RV variations. If the surface spot is responsible for RV variations, both values should coincide or should be a multiples of rotation period if the number of spots is

multiple. This controversy can be solved if the values of rotation period is underestimated in our work.

Thus, while we found a correlation in variations of BVS and RV data but could not prove these variations in other surface activity indicators we cannot reject safely the exoplanet hypothesis as a reason of RV variations. More continuous observations have to be undertaken to clear the nature of long-term periodic RV variations in α Ari.

Accepting at this moment the observed RV of 395-day variations is caused by an orbiting companion the exoplanet hypothesis let's look is it in agreement with other parameters for orbit.

The determined orbit is quite eccentric: $e = 0.25 \pm 0.02$. Up to now, 4 out of 13 companions around K-giants show more than 0.2 eccentricity: $e = 0.7$ of ι Dra (Frink et al. 2002), $e = 0.2$ of K1III giant HD 47536 (Setiawan et al. 2003), $e = 0.27$ of K1II-III giant HD 13189 (Hatzes et al. 2005), and $e = 0.43$ of K1III giant 4 UMa (Döllinger et al. 2007). Hence, $e = 0.25$ of α Ari is not unusual among K-giants and such quite eccentric modulation is difficult to be produced by surface variations or stellar oscillations.

α Ari is a K-giant of stellar mass of $M_\star = 1.4$–$5.6\ M_\odot$ and radius of $R_\star = 13.9\ R_\odot$. To date there are just two companions detected in more massive stars than α Ari: namely HD 13189 with 2–7 $M_\odot$ (Hatzes et al. 2005) and NGC 4349 No. 127 with 3.9 $M_\odot$ (Lovis & Mayor 2007). They have the minimum masses of 8–20 and 19.8 M_{Jup}, respectively. They are

classified as brown dwarfs because they are beyond definition of planet ($m \sin i \leq 13$ M_{Jup}).

Hence, if the companion is present in K-giant α Ari it is the most massive star with a large stellar radius around which a planetary companion has been discovered (Figure 4.10) and having also multi-periodic oscillations.

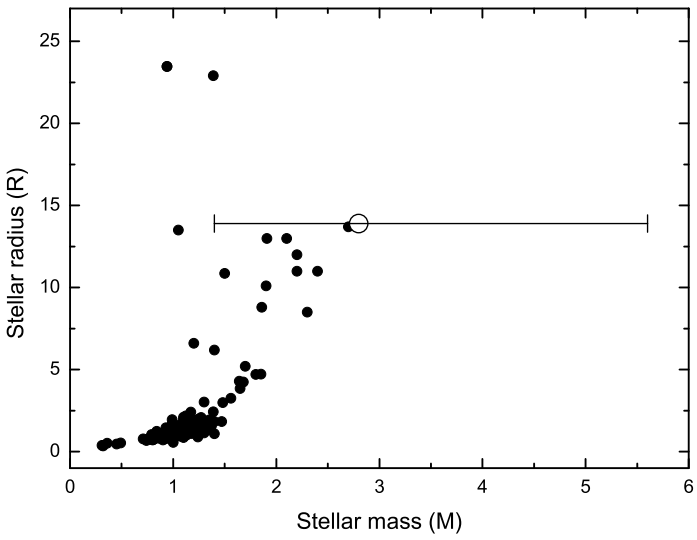

Figure 4.10: Stellar mass vs. radius distribution of stars with known planetary companions (as of November 2008). Open circle and a horizontal line indicate a mean mass and a possible mass limit of α Ari.

References

Allende Prieto, C., & Lambert, D. L. 1999, A&A, 352, 555

Berdyugina, S. V., Boyarchuk, M. E., Pavlenko, Y. V., et al. 1991, Soviet Astronomy, 35, 387

Carney, B. W., Gray, D. F., Yong, D., et al. 2008, AJ, 135, 892

Döllinger, M. P., Hatzes, A. P., Pasquini, L., et al. 2007, A&A, 472, 649

Evans, D. S., 1967, IAUS, 30, 57

Frink, S., Mitchell, D. S., Quirrenbach, A., et al. 2002, ApJ, 576, 478

Gray, D. F., Scott, H. R., & Postma, J. E. 2002, PASP, 114, 536

Han, I., Kim, K.-M., Lee, B.-C., et al. 2007, Publication of Korean Astronomical Society, 22, 75

Hatzes, A. P., Guenther, E. W., Endl, M., et al. 2005, A&A, 437, 743

Hatzes, A. P., Cochran, W. D., Endl, M., et al. 2006, A&A, 457, 335

Hekker, S., & Meléndez, J. 2007, A&A, 475, 1003

Johnson, J. A., Fischer, D. A., Marcy, G. W., et al. 2007, ApJ, 665, 785

Johnson, J. A., Marcy, G. W., Fischer, D. A., et al. 2008, ApJ, 675, 784

Kim, K. M., Mkrtichian, D. E., Lee, B.-C., et al. 2006, A&A, 454, 839

Kim, K.-M., Han, I., Valyavin, G. G., et al. 2007, PASP, 119, 1052

Kürster, M., Endl, M., Rouesnel, F., et al. 2003, A&A, 403, 1077

Larson, A. M., Yang, S. L. S., & Walker, G. A. H. 1999, IAU Colloq. 170: Precise Stellar Radial Velocities, 185, 193

Lovis, C., & Mayor, M. 2007, A&A, 472, 657

Mayor, M., & Queloz, D. 1995, NATURE, 378, 355

Mitchell, D. S., Frink, S., Quirrenbach, A., et al. 2003, Bulletin of the American Astronomical Society, 35, 1234

Mozurkewich, D., Johnston, K. J., Simon, R. S., et al. 1991, AJ, 101, 2207

Piskunov, N. E., Kupka, F., Ryabchikova, T. A., et al. 1995, A&AS, 112, 525

Queloz, D., Henry, G. W., Sivan, J. P., et al. 2001, A&A, 379, 279

Reffert, S., Quirrenbach, A., Mitchell, D. S., et al. 2006, ApJ, 652, 661

Reiners, A., & Royer, F. 2004, A&A, 428, 199

Sato, B., Izumiura, H., Toyota, E., et al. 2007, ApJ, 661, 527

Sato, B., Izumiura, H., Toyota, E., et al. 2008, PASJ, 60, 539

Setiawan, J., Hatzes, A. P., von der Lühe, O., et al. 2003, A&A, 398, L19

Setiawan, J. 2003, Earths: DARWIN/TPF and the Search for Extrasolar Terrestrial Planets, 539, 595

Tody, D. 1986, "The IRAF Data Reduction and Analysis System" in Proc. SPIE Instrumentation in Astronomy VI, ed. D. L. Crawford, 627, 733

Walker, G. A. H., Yang, S., Campbell, B., et al. 1989, ApJL, 343, L21

Chapter 5

Summary

In 1990s, developments of high-resolution spectrograph created a study of a low-amplitude stellar oscillation. However, it is still an unexplored field because such instruments are not widely available.

After development of a high-resolution echelle spectrograph, Bohyunsan Observatory Echelle Spectrograph (BOES) at Bohyunsan Optical Astronomy Observatory (BOAO) in 2003, we could finally seize an opportunity to research precise radial velocity (RV) measurements. The maximum efficiency of the BOES is close to 12 % including the light loss due to the atmospheric extinction, the reflectance of the telescope, and the light cutoff at the fiber input (Kim et al. 2007). Compared to the efficiencies of other high-resolution spectrographs for $\sim$ 2 m class telescopes, the efficiency of the BOES is a lot better in the world. The BOES also has been maintained at stable condition for seven years with an actual accuracy of approximately 7 m s^{-1}.

There are two main research programs using BOES: such of an internal variability such as 'Spectral atlases' and an external variability such as 'Exoplanet detections'. Most of exoplanet detection by precise RV measurement programs is mainly looking for companions or study of planet formation around F-, G-, and K-dwarfs. Because giants and supergiants are believed to be active and in messy state in the region of the Hertzsprung-Russell (H-R) diagram, in many cases of precise RV observations of giant and supergiant a spectrum is mixed mainly by three components, pulsation, rotational modulation by surface structure, or

low-mass companion. It seems that majority of spectra are blended with two kinds of components and contain the rotational velocity of the star, which makes it difficult to understand what kind of pulsations might cause these RV variations. It is also very hard to extract the RV components from the original spectrum, and the nature of the long-period RV variations is still open to debate. Thus, both exoplanet detection and asteroseismic investigation could be carried out with precise RV measurement. For giants, Sato et al. (2003) already has been carrying out exoplanet detection around G-giants and the first results of K-giant survey are reported by Frink et al. (2002).

Since 2004, we obtained early and bright 55 K-giants and supergiants (and several F-, and M-giants and supergiants), and 30 chemically peculiar Ap stars for the program 'Exoplanet Detection and Asteroseisimic Study of K-giants and Ap Stars'. It was designed to avoid overlap with other exoplanet search programs. An RV accuracy of ~ 10 m s^{-1} achieved with BOES is good enough to detect planetary companions (Omiya et al. 2008). As our first result of the survey program, multi-periodic oscillations in α Arietis were detected by Kim et al. (2006). We have found in total nine exoplanet candidates from 55 K-giants and supergiants showing long-term periodic RV variations (Han et al. *in preparation*). On the other hand, we did not find any short period planet candidate, which is quite natural because the radii of the giant stars are typically as large as 10 $R_\odot$. Recently, one of them, γ^1 Leonis (HD 89484; K0 III, V =

2.01), was discovered to harbor a planetary companion with $m \sin i$ = 8.78 M_J (Han et al. 2010) orbiting a host star with a mass of 1.23 $M_\odot$. The survey indicates about 60 % of the target stars have variable RV and about 20 % of the list shows well defined periodic variation compatible with orbital motion. Actually, the detection rate around K-giants and supergiants agrees well with the results of other survey (Pasquini et al. 2008) that reports at least 10 % detection rate around giants. It is reported that the giants with confirmed exoplanet do not show a tendency of high metallicity in contrast to the dwarf stars with exoplanet. We did not estimate the metallicity of our exoplanet candidate stars. It remains as a future work.

In this thesis, we present a spectral atlas for F5 Ib α Persei and precise RV measurements of two stars for F7 Ib Polaris and K2 III α Arietis.

First, we present a high-resolution spectral atlas of the F5 Ib star α Persei (HD 20902) with a synthetic spectrum and line identification tables. The spectral atlas of α Persei is compared with a synthetic spectrum computed using a code based on Kurucz software and databases. The spectral lines of α Persei have been identified by matching the synthetic spectrum with the observed one. All data can be downloading in digital form on the web. We hope that the spectral atlas provides useful information for future studies as an example of high-quality spectrum of a F5 Ib star.

Second, we present precise RV variations of F7 Ib Polaris and K2

III α Arietis. Polaris shows remarkable changes in the amplitude and the period of pulsations that occurred at the end of the 20th and the beginning of the 21st century. We also detected a 119 day secondary RV variation which is about three times longer than previously reported results. It is concluded that the 119 day variation is not coherent on long timescales and have discussed the possible nature of these variations. α Arietis shows a low-amplitude of a 395-day RV variations. Although we do not find the correlation between RV variations and equivalent widths (EWs) of chromospheric activity indicators (H_α and CaII 8662 Å line), bisector analysis indeed shows that bisector velocity span (BVS) and RV variations are strongly correlated with each other, while we do not find the 395-day period in variations in BVS. It is difficult to answer weather the RV variations are produced by intrinsic changes of shapes of spectral lines due to surface spots or by a companion. We cannot indeed safely reject the exoplanet hypothesis as reason of at least part of RV variations.

A continuous survey is needed to confirm the RV periodicity of the candidates and to determine their orbital parameters. It will be utilized in the studies of a nature and a cause of the RV variation of giants and supergiants (their elemental abundances, physical parameters, and eventually their evolutionary status), which would also help to understand the planet formation mechanisms.

References

Frink, S., Mitchell, D. S., Quirrenbach, A., Fischer, D. A., Marcy, G. W., & Butler, R. P. 2002, ApJ, 576, 478

Han, I. et al., *in preparation*

Han, I., Lee, B. C., Kim, K. M., Mkrtichian, D. E., Hatzes, A. P., & Valyavin, G. 2010, A&A, 509, A24

Kim, K. M., Mkrtichian, D. E., Lee, B.-C., Han, I., & Hatzes, A. P. 2006, A&A, 454, 839

Kim, K.-M., Han, I., Valyavin, G. G., Plachinda, S., Jang, J. G., Jang, B.-H. et al. 2007, PASP, 119, 1052

Omiya, M., Izumiura, H., Han, I., Lee, B.-C., Sato, B., Kambe, E., Kim, K.-M., Yoon, T. S. et al. 2009, PASJ, 61, 825

Pasquini, L., Doellinger, M. P., Hatzes, A., Setiawan, J., Girardi, L., da Silva, L., & de Medeiros, J. R. 2008, arXiv:0801.3336

Sato, B., Ando, H., Kambe, E., Takeda, Y., Izumiura, H., Masuda, S., Watanabe, E., Noguchi, K. et al. 2003, ApJL, 597, L157

Appendix A

Atlas of α Persei

A.1 Whole atlas and synthetic spectrum

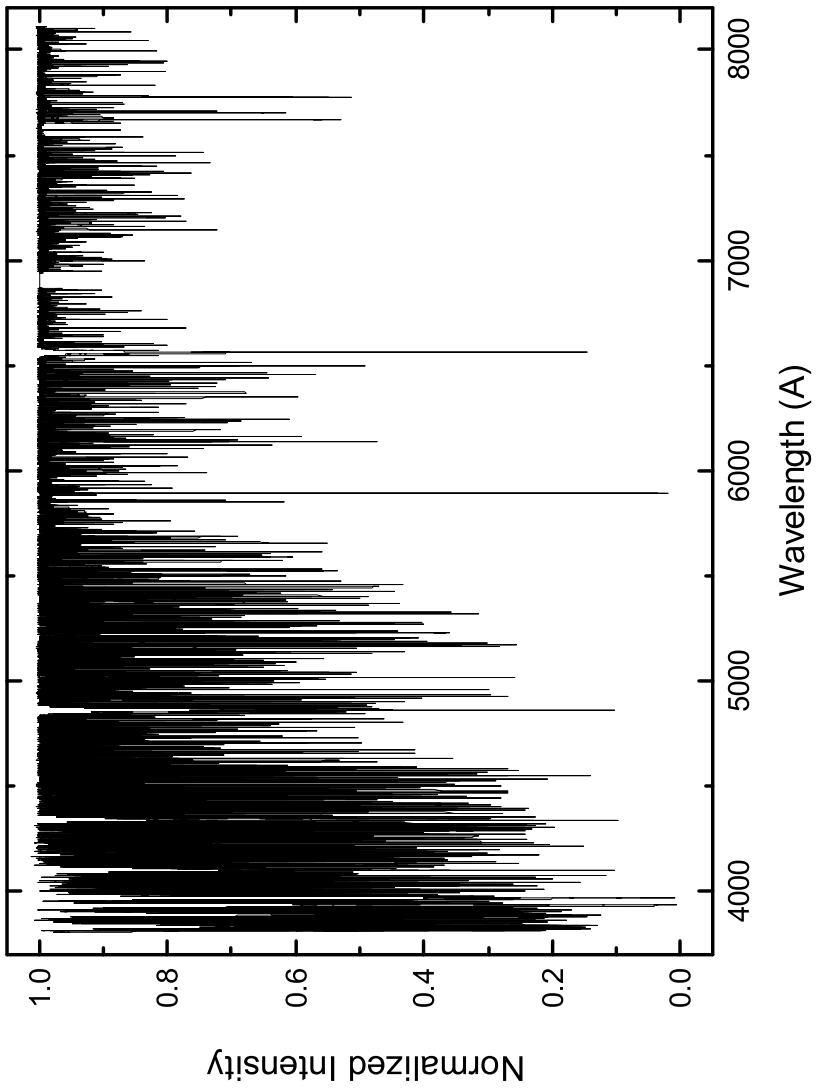

Figure A.1: Whole spectral atlas of the F5Ib star α Per covering the 3810–8100 Å region.

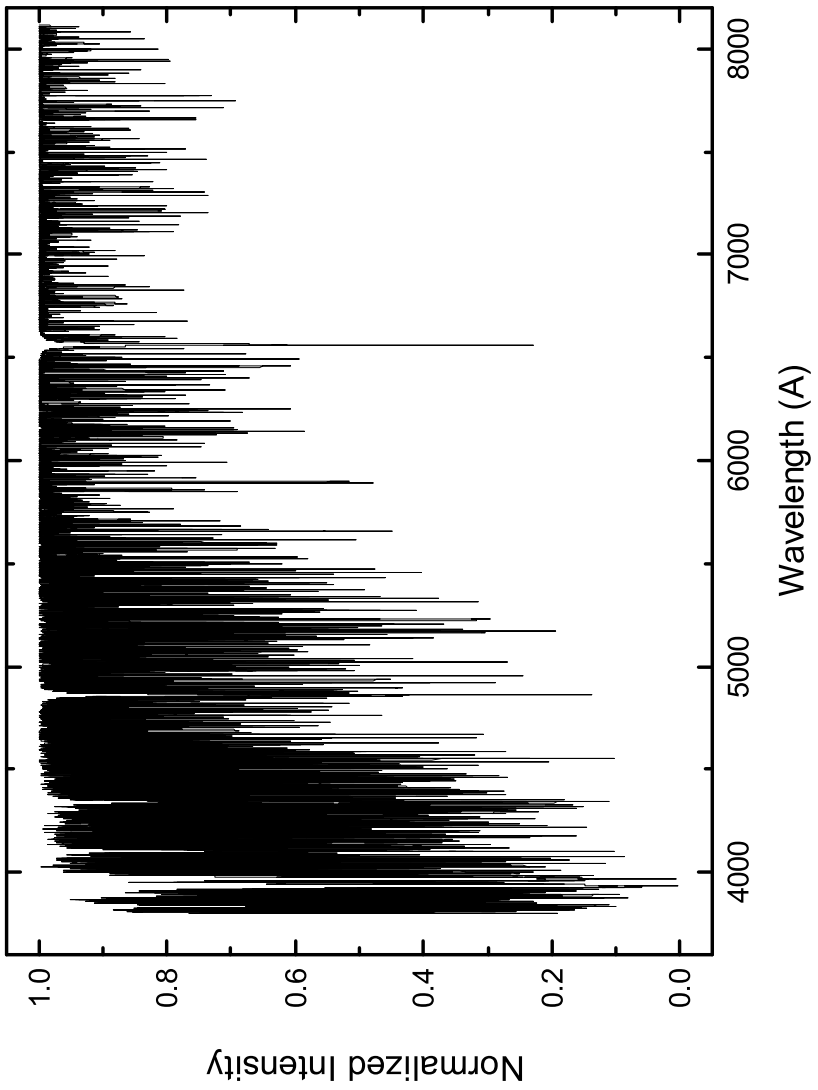

Figure A.2: Whole synthetic spectrum of the F5Ib star α Per covering the 3810–8100 Å region.

A.2 Line tables and figures

The complete line tables and figures are downloadable in digital form on the WWW of the BOhyunsan observatory[1]

Identification lists:

aper-lines - lines list (all lines used for calculations)

aper-lines-non-zero - existing lines list

aper-lines-stronger–1-percent - list of lines deeper than 1%

aper-lines-stronger-10-percent - list of lines deeper than 10%

T06240g0p580.mod - atmosphere model

Columns description:

(a) wavelength

(b) identification

(c) Kurucz code (for example, FeII=26.01, CN=607.00)

(d) Line depth in percent*10

(e) Depth of synthetic spectrum ($\times$ 1000)

(without rotation and instrumental profile) at this wavelength)

Absolute depth of a line = ((e)/1000) $\times$ ((d)/1000)

Each piece of spectral figures is shown twice in a single panel with different scales: one is shown in the whole intensity scale, while the other is shown with magnification factor of 20.

[1] http://boao.kasi.re.kr/BOES/atlas/hd20902.html

Appendix B

List of program stars

Table B.1: List of atlases

HD	Name	V	E(B-V)	RA(2000)	Dec(2000)	Sp. type
47839	15 S Mon	4.660	0.070	6 40 58.66	+09 53 44.7	O7 V
214680	10 Lac	4.877	0.106	22 39 15.68	+39 03 01.0	O9 V
36512	upsilon Ori	4.620	0.040	5 31 55.86	-07 18 05.5	B0 V
37128	epsilon Ori	1.700	0.040	5 36 12.81	-01 12 06.9	B0 Iab
41117	chi-2 Ori	4.646	0.370	6 3 55.18	+20 08 18.4	B2 Ia
206165	9 Cep	4.788	0.399	21 37 55.22	+62 04 55.0	B2 Ib
120315	eta UMa	1.852	0.103	13 47 32.44	+49 18 47.8	B3 V
32630	eta Aur	3.158	0.054	5 6 30.89	+41 14 04.1	B3 V
53138	omicron2 Cma	3.000	0.060	7 3 1.47	-23 49 59.8	B3 Ia
58350	eta CMa	2.400	0.070	7 24 5.7	-29 18 11.2	B5 Iab
34085	beta Ori	0.120	0.000	5 14 32.27	-08 12 05.9	B8 Iab
103287	gamma UMa	2.427	0.061	11 53 49.85	+53 41 41.1	A0 V
172167	alpha Lyr	0.030	0.020	18 36 56.34	+38 47 01.3	A0 V
87737	eta Leo	3.511	-0.017	10 7 19.95	+16 45 45.6	A0 Ib
21389	+58 607	4.600	0.453	3 29 54.74	+58 52 43.5	A0 Ia
197345	alpha Cyg	1.250	0.060	20 41 25.91	+45 16 49.2	A2 Ia
216956	alpha PsA	1.160	0.010	22 57 39.05	-29 37 20.1	A3 V
89025	zeta Leo	3.443	0.030	10 16 41.42	+23 25 02.3	F0 III
36673	alpha Lep	2.597	0.030	5 32 43.82	-17 49 20.2	F0 Ib
113139	78 UMa	4.930	0.010	13 0 43.7	+56 21 58.8	F2 V
20902	alpha Per	1.816	0.150	3 24 19.37	+49 51 40.2	F5 Iab
30652	pi-3 Ori	3.190	-0.020	4 49 50.41	+06 57 40.6	F6 V
194093	gam Cyg	2.237	0.101	20 22 13.7	+40 15 24.0	F8 Iab
54605	delta CMa	1.842	0.112	7 8 23.48	-26 23 35.5	F8 Iab
109358	beta CVn	4.260	0.010	12 33 44.54	+41 21 26.9	G0 V
121370	eta Boo	2.680	-0.030	13 54 41.08	+18 23 51.8	G0 IV
204867	beta Aqr	2.910	0.070	21 31 33.53	-05 34 16.2	G0 Ib
20630	kappa Cet	4.830	0.000	3 19 21.7	+03 22 12.7	G5 V
161797	mu Her	4.410	-0.010	17 46 27.53	+27 43 14.4	G5 IV
206859	9 Peg	4.344	0.147	21 44 30.7	+17 21 00.1	G5 Ib
101501	61 UMa	4.320	-0.010	11 41 3.02	+34 12 05.9	G8 V
188512	beta Aql	3.710	0.020	19 55 18.79	+06 24 24.3	G8 IV
62345	kappa Gem	3.570	-0.010	7 44 26.85	+24 23 52.8	G8 III
113226	epsilon Vir	2.830	0.000	13 2 10.6	+10 57 32.9	G8III(Ib)
48329	epsilon Gem	3.019	0.289	6 43 55.93	+25 07 52.0	G8Ib

Table B.1: continued.

HD	Name	V	E(B-V)	RA(2000)	Dec(2000)	Sp. type
185144	sigma Dra	4.700	-0.040	19 32 21.59	+69 39 40.2	K0 V
62509	beta Gem	1.150	0.000	7 45 18.95	+28 01 34.3	K0 III
197989	epsilon Cyg	2.500	-0.010	20 46 12.68	+33 58 12.9	K0 III
222404	gamma Cep	3.225	0.072	23 39 20.85	+77 37 56.2	K1 IV
22049	epsilon Eri	3.730	-0.030	3 32 55.84	-09 27 29.7	K2 V
12929	alpha Ari	2.000	-0.010	2 7 10.41	+23 27 44.7	K2 III
153210	kappa Oph	3.200	-0.010	16 57 40.1	+09 22 30.1	K2 III
127665	rho Boo	3.583	0.046	14 31 49.79	+30 22 17.2	K3 III
31398	iota Aur	2.693	0.152	4 56 59.62	+33 09 57.9	K3 II
201091	61 Cyg A	5.210	0.030	21 6 53.94	+38 44 57.9	K5 V
164058	gamma Dra	2.230	0.020	17 56 36.37	+51 29 20.0	K5 III
6860	beta And	2.060	0.020	1 9 43.92	+35 37 14.0	M0 III
1013	chi Peg	4.818	-0.025	0 14 36.16	+20 12 24.1	M2 III
39801	alpha Ori	0.580	0.090	5 55 10.31	+07 24 25.4	M2 Ib
206936	mu Cep	4.040	0.550	21 43 30.46	+58 46 48.2	M2 Ia

Table B.2: List of Ap stars

HD	V	Sp. type	P_{rot} (d)	RA(2000)	Dec(2000)
2453	6.9	A2p	?	00 28 28.57	+32 26 15.90
8441	6.7	A2Sr	69.43	01 24 18.67	+43 08 31.55
12288	7.7	A0p	?	02 03 30.51	+69 34 56.40
26571	6.2	B8Si	15.7	04 12 51.24	+22 24 48.45
42616	7.2	A1SrCrEu	17	06 00 58.56	+47 54 06.92
40394	5.7	A0SiFe	14.37	06 00 58.56	+47 54 06.92
43819	6.3	B9Si9Si	15.03	06 19 01.84	+17 19 30.93
62140	6.5	F0p	4.23	07 46 27.41	+62 49 49.90
65339	6.0	A2p	8.03	08 01 42.45	+60 19 27.67
71866	6.7	A1EuSrCr	6.8	08 31 10.64	+40 13 29.60
74521	5.6	A1p	7.7	08 44 45.04	+10 04 54.00
90994	5.1	B6p	15	10 30 17.47	–00 38 13.29
111133	6.3	A1SrCrEu	16.3	12 47 02.30	+05 57 01.34
112413	2.9	A0p	5.5	12 56 01.66	+38 19 06.17
118022	4.9	A1p	3.72	13 34 07.93	+03 39 32.28
125248	5.8	A2p	130	14 18 38.00	–18 42 57.00
126515	7.1	A2pEuCr	130	14 25 55.88	+00 59 33.80
134214	7.5	roAp	?	15 09 02.41	–13 59 58.70
137909	3.7	F0p	18.5	15 27 49.73	+29 06 20.53
137949	6.8	roAp	?	15 29 35.00	–17 26 27.00
170973	6.4	A0SiCrSr	18.1	18 32 06.88	+03 39 34.57
173650	6.5	A0SiCrSr	9.97	18 45 35.61	+21 59 04.85
188041	5.6	A5p	224	19 53 18.74	–03 06 52.10
192678	7.3	A4p	6.42	20 13 36.32	+53 39 33.55
192913	6.6	A0SiCr	16.8	20 16 27.20	+27 46 33.86
196502	5.2	A2SrCrEu	20.27	20 31 30.41	+74 57 16.63
137909	3.7	F0p	?	15 27 49.73	+29 06 20.50
200311	7.7	B9p	52	21 01 14.32	+43 43 18.43
201601	4.7	FOp	75yr	21 10 20.50	+10 07 53.70
221568	7.6	A0pSrCrEu	79.5	23 32 47.64	+57 54 20.10

Table B.3: List of K-giants and supergiants

HR	Name	V	B-V	Abs V	RA(2000)	Dec(2000)	Sp. type
164		5.45	1.69	-2.62	00 39 09.8941	+49 21 16.519	K7 III
165	31 And	3.28	1.28	0.81	00 39 19.6758	+30 51 39.686	K3 III
168	Alp Cas	2.25	1.18	-1.98	00 40 30.4405	+56 32 14.392	K0 IIIa
224	Del Psc	4.44	1.52	-0.43	00 48 40.9443	+07 35 06.285	K4 IIIb
285		4.24	1.24	-0.66	01 08 44.8773	+86 15 25.52	K2 II-III
617	Alp Ari	2.00	1.15	-1.53	02 07 10.4071	+23 27 44.723	K2 III
941	Kap Per	3.80	0.98	1.11	03 09 29.7715	+44 51 27.157	K0 III
947	Ome Per	4.61	1.12	-0.22	03 11 17.3816	+39 36 41.697	K1 III
999		4.47	1.60	-2.00	03 20 20.3608	+29 02 54.450	K2 II-III
1052	Sig Per	4.35	1.40	-0.82	03 30 34.4835	+47 59 42.778	K3 III
1411	77 Tau	3.85	0.94	0.42	04 28 34.4959	+15 57 43.851	K0 III
1457	Alp Tau	0.85	1.54	-0.65	04 35 55.2387	+16 30 33.485	K5 III
1577	Iot Aur	2.69	1.55	-3.29	04 56 59.6187	+33 09 57.925	K3 II
1907	Phi2 Ori	4.09	0.95	1.33	05 36 54.3879	+09 17 26.422	K1 III
2503	17 Mon	4.78	1.42	-1.08	06 47 19.8306	+08 02 14.114	K4 III
2990	Bet Gem	1.15	1.00	1.08	07 45 18.9503	+28 01 34.315	K0 IIIb
3145		4.40	1.27	-0.12	08 02 15.9369	+02 20 04.454	K2 III
3249	Bet Cnc	3.54	1.51	-1.21	08 16 30.9206	+09 11 07.961	K4 III
3461	Del Cnc	3.94	1.08	0.84	08 44 41.0996	+18 09 15.511	K9 III-II
3731	Kap Leo	4.47	1.24	0.39	09 24 39.2591	+26 10 56.36	K2 III
3748	Alp Hya	2.00	1.49	-1.68	09 27 35.2433	-08 39 30.969	K3 II-III
3751		4.27	1.52	-3.32	09 37 05.2871	+81 19 34.97	K3 IIIa
3773	Lam Leo	4.31	1.56	-0.77	09 31 43.2281	+22 58 04.694	K5 III
3905	Mu Leo	3.88	1.22	0.83	09 52 45.8173	+26 00 25.02	K2 III
4057	Gam LeoA	2.61	1.15	-0.32	10 19 58.427	+19 50 28.5	K1 III
4301	Alp UMa	1.79	1.07	-1.10	11 03 43.6687	+61 45 03.72	K0 Iab
4737	Gam Com	4.35	1.14	0.74	12 26 56.2723	+28 16 06.322	K1 III
4954	41 Com	4.80	1.50	-0.04	13 07 10.7297	+27 37 29.067	K5 III
5219		4.77	1.65	-1.57	13 51 47.4751	+34 26 39.26	K5 III
5340	Alp Boo	-0.04	1.23	-0.30	14 15 39.6720	+19 10 56.677	K1.5 III
5616	Psi Boo	4.52	1.28	0.10	15 04 26.7417	+26 56 51.536	K2 III
5744	iota Dra	3.31	1.18	0.83	15 24 55.7747	+58 57 57.836	K2 III
5854	Alp Ser	2.64	1.18	0.88	15 44 16.0749	+06 25 32.257	K2 III
5947	Eps CrB	4.14	1.25	-0.10	15 57 35.2518	+26 52 40.36	K2 III
6159	29 Her	4.84	1.49	-0.10	16 32 36.2921	+11 29 16.949	K7 III

Table B.3: continued.

HR	Name	V	B-V	Abs V	RA(2000)	Dec(2000)	Sp. type
6299	Kap Oph	3.20	1.15	1.10	16 57 40.0973	+09 22 30.118	K2 III
6418	Pi Her	3.16	1.44	-2.10	17 15 02.8343	+36 48 32.98	K3 Iab
6498	Sig Oph	4.34	1.51	-3.44	17 26 30.8803	+04 08 25.295	K2 II
6705	Gam Dra	2.23	1.52	-1.05	17 56 36.3699	+51 29 20.02	K5 III
6746	Gam Sge	2.99	1.00	0.64	18 05 48.4869	-30 25 26.729	K0 III
6859	Del Sgr	2.71	1.42	-2.16	18 20 59.6417	-29 49 41.172	K3 IIIa
6869	Eta Ser	3.26	0.94	1.87	18 21 18.6007	-02 53 55.770	K0 III-IV
6872	Kap Lye	4.32	1.18	0.01	18 19 51.7095	+36 03 52.371	K2 III
7417	Bet Cyg	3.08	1.09	-2.28	19 30 43.2806	+27 57 34.852	K3 III
7525	Gam Aql	2.72	1.58	-3.03	19 46 15.5795	+10 36 47.740	K3 II
7615	Eta Cyg	3.91	1.00	0.75	19 56 18.3719	+35 05 00.325	K0 III
7957	Gam Del	4.27	1.04	1.80	20 46 39.5023	+16 07 27.466	K0 IV
8173	1 Peg	4.09	1.11	0.72	21 22 05.1996	+19 48 16.229	K1 III
8308	Eps Peg	2.40	1.56	-4.17	21 44 11.1581	+09 52 30.041	K2 Ib
8465	Zet Cep	3.36	1.59	-3.38	22 10 51.2767	+58 12 04.539	K1.5 Ib
8485		4.51	1.39	-1.68	22 13 52.7300	+39 42 53.737	K3 III
8916	10 Psc	4.28	1.07	0.95	23 27 58.0951	+06 22 44.372	K1 III

Appendix C

RV measurements of program stars

Table C.1: RV measurements for Polaris during November 2004 and June 2007

JD-2450000 day	ΔRV $km\,s^{-1}$	$\pm\sigma$ $km\,s^{-1}$	JD-2450000 day	ΔRV $km\,s^{-1}$	$\pm\sigma$ $km\,s^{-1}$	JD-2450000 day	ΔRV $km\,s^{-1}$	$\pm\sigma$ $km\,s^{-1}$	JD-2450000 day	ΔRV $km\,s^{-1}$	$\pm\sigma$ $km\,s^{-1}$
3332.939450	0.265	0.015	3818.370454	1.338	0.019	3985.293499	1.133	0.015	4225.322176	-1.186	0.014
3332.943628	0.245	0.013	3818.375011	1.335	0.018	3985.360099	1.174	0.015	4225.324549	-1.177	0.014
3333.395349	0.949	0.034	3819.088512	1.061	0.018	4006.975176	-0.677	0.017	4225.955700	-1.378	0.017
3333.400025	0.990	0.021	3819.092702	1.063	0.016	4007.106878	-0.781	0.018	4225.963107	-1.347	0.016
3333.963866	1.479	0.018	3819.349578	0.636	0.016	4008.313199	0.329	0.018	4225.970514	-1.351	0.015
3333.969457	1.499	0.016	3819.356603	0.642	0.016	4008.317979	0.338	0.018	4225.977921	-1.350	0.013
3333.974897	1.480	0.017	3820.079167	-0.573	0.021	4008.366581	0.424	0.018	4225.985340	-1.343	0.018
3333.988392	1.499	0.017	3820.088021	-0.565	0.017	4008.370783	0.432	0.019	4225.995965	-1.338	0.015
3333.993693	1.501	0.016	3821.036895	-0.653	0.017	4011.181866	-0.818	0.016	4225.995965	-1.337	0.015
3334.269832	1.447	0.016	3821.043376	-0.660	0.013	4012.032284	-0.148	0.017	4226.010895	-1.326	0.013
3334.273606	1.429	0.015	3821.182919	-0.489	0.013	4012.355604	0.377	0.018	4226.018510	-1.318	0.013
3334.277043	1.444	0.017	3821.189215	-0.481	0.015	4012.366245	0.396	0.017	4226.026068	-1.293	0.016
3334.280481	1.448	0.017	3821.372240	-0.200	0.016	4014.942951	-0.813	0.017	4226.044308	-1.235	0.026
3353.928598	1.072	0.014	3821.377217	-0.122	0.015	4015.375783	-0.908	0.018	4226.051716	-1.272	0.024
3353.932973	1.065	0.015	3822.183527	0.983	0.019	4017.926503	0.683	0.018	4227.958005	0.883	0.014
3506.118579	-0.345	0.011	3822.190760	0.968	0.016	4017.931341	0.661	0.017	4227.962519	0.885	0.015
3506.123984	-0.358	0.011	3823.982058	-0.631	0.014	4018.035280	0.492	0.018	4228.947574	-0.641	0.013
3507.240093	-0.647	0.009	3823.987772	-0.641	0.013	4202.934088	-0.166	0.020	4228.951219	-0.645	0.014
3507.243855	-0.632	0.008	3831.151079	0.651	0.013	4202.937201	-0.168	0.019	4229.272519	-1.103	0.025
3507.247292	-0.632	0.009	3831.158370	0.631	0.011	4202.940800	-0.168	0.018	4229.287298	-1.158	0.013
3507.250730	-0.633	0.009	3833.980635	0.748	0.014	4203.138814	0.201	0.022	4229.295435	-1.171	0.014
3510.055821	-0.258	0.011	3833.987602	0.732	0.011	4204.933655	-0.215	0.019	4230.952776	0.231	0.014
3510.073981	-0.273	0.011	3841.290294	-0.198	0.012	4204.935970	-0.222	0.017	4230.955820	0.233	0.015
3519.295729	-0.283	0.013	3867.086904	0.385	0.014	4205.157061	-0.632	0.018	4230.958273	0.228	0.016
3534.190258	-0.535	0.015	3867.092448	0.373	0.010	4205.160337	-0.630	0.015	4230.960368	0.239	0.014
3534.193846	-0.551	0.013	3877.082759	0.021	0.015	4207.056935	0.149	0.022	4231.320081	0.785	0.016
3534.197492	-0.550	0.015	3877.088303	0.028	0.014	4207.061171	0.156	0.021	4231.322975	0.808	0.014
3534.201173	-0.570	0.014	3877.093291	0.040	0.015	4208.988579	-0.376	0.023	4234.324176	-0.770	0.018
3536.235296	1.116	0.018	3877.098152	0.028	0.014	4209.106167	-0.644	0.024	4235.985246	1.021	0.023
3536.239220	1.139	0.018	3877.103060	0.049	0.013	4209.980442	-1.369	0.019	4235.988406	1.028	0.019
3543.060704	-0.637	0.015	3877.108025	0.047	0.014	4210.121456	-1.300	0.016	4235.990952	1.002	0.023
3543.064963	-0.647	0.014	3888.014715	-0.622	0.020	4210.125322	-1.272	0.020	4238.317301	-0.728	0.015
3543.069847	-0.631	0.017	3888.019634	-0.603	0.021	4210.250965	-1.147	0.016	4238.319859	-0.719	0.014

Table C.1: continued.

JD-2450000 day	ΔRV $km\,s^{-1}$	$\pm\sigma$ $km\,s^{-1}$	JD-2450000 day	ΔRV $km\,s^{-1}$	$\pm\sigma$ $km\,s^{-1}$	JD-2450000 day	ΔRV $km\,s^{-1}$	$\pm\sigma$ $km\,s^{-1}$	JD-2450000 day	ΔRV $km\,s^{-1}$	$\pm\sigma$ $km\,s^{-1}$
3543.075762	-0.640	0.016	3888.113163	-0.641	0.016	4210.329134	-1.066	0.022	4240.961829	-0.652	0.013
3700.293243	0.430	0.020	3888.244608	-0.620	0.019	4213.294403	-0.959	0.020	4240.965070	-0.638	0.016
3700.296993	0.426	0.016	3888.319005	-0.587	0.016	4213.963443	-1.391	0.016	4241.311151	-1.117	0.015
3700.983173	-0.687	0.015	3888.994125	0.213	0.018	4214.056842	-1.338	0.020	4241.313709	-1.104	0.014
3700.989261	-0.673	0.017	3889.108695	0.413	0.020	4214.966384	0.002	0.020	4241.982642	-1.125	0.014
3700.994689	-0.693	0.017	3889.113892	0.413	0.019	4214.970643	0.031	0.018	4241.985848	-1.131	0.014
3701.000326	-0.703	0.016	3889.248068	0.642	0.020	4215.946688	1.028	0.017	4241.987700	-1.125	0.014
3729.357727	-0.886	0.019	3891.102342	0.543	0.020	4215.949338	1.032	0.016	4242.953688	0.368	0.015
3729.362148	-0.881	0.018	3891.256073	0.255	0.021	4216.326421	0.686	0.017	4242.956628	0.364	0.016
3729.367357	-0.892	0.017	3895.984324	-0.732	0.016	4216.329464	0.681	0.017	4243.314747	0.850	0.017
3729.373005	-0.862	0.017	3895.988479	-0.734	0.017	4216.942002	-0.397	0.016	4243.316969	0.847	0.017
3730.391115	0.324	0.018	3896.258304	-0.693	0.016	4216.944722	-0.410	0.015	4249.289750	-1.154	0.016
3730.396797	0.342	0.018	3896.262899	-0.693	0.016	4217.942179	-1.387	0.015	4249.292204	-1.153	0.015
3751.377138	1.082	0.012	3898.001730	1.490	0.018	4217.948105	-1.411	0.015	4251.098497	0.740	0.018
3751.381895	1.076	0.012	3898.189484	1.486	0.018	4218.334099	-1.069	0.017	4251.102016	0.747	0.018
3751.386316	1.081	0.011	3898.305791	1.450	0.018	4218.338305	-1.049	0.013	4251.274583	0.945	0.019
3756.301670	-0.177	0.013	3899.094479	0.298	0.015	4218.954589	0.007	0.016	4252.211353	0.639	0.039
3756.306924	-0.183	0.012	3899.322556	-0.074	0.016	4218.957124	0.028	0.015	4252.217429	0.608	0.022
3758.293478	0.637	0.015	3980.046273	-0.755	0.015	4219.949384	0.984	0.015	4254.973553	0.609	0.017
3758.298130	0.652	0.016	3980.055590	-0.750	0.015	4219.952648	0.970	0.014	4254.973206	0.827	0.016
3760.927096	-0.741	0.014	3980.193443	-0.536	0.015	4220.330727	0.631	0.019	4255.168273	0.893	0.018
3760.931437	-0.729	0.015	3980.294615	-0.361	0.016	4222.980843	0.044	0.014	4262.172851	-0.664	0.017
3761.921389	0.152	0.019	3980.302405	-0.364	0.015	4222.983413	0.051	0.015	4262.176185	-0.676	0.015
3761.927373	0.179	0.018	3980.988279	0.774	0.016	4223.076558	0.218	0.014	4262.310096	-0.485	0.018
3778.112610	0.660	0.019	3980.993565	0.778	0.017	4223.079278	0.221	0.015	4263.025508	0.739	0.020
3778.370368	1.026	0.017	3981.029169	0.827	0.016	4223.965352	0.921	0.017	4263.152498	0.890	0.020
3778.375796	1.037	0.017	3981.033393	0.822	0.015	4223.970490	0.914	0.017	4263.307601	1.034	0.023
3779.919229	0.203	0.014	3981.161199	0.964	0.017	4224.098230	0.808	0.015	4264.042979	0.782	0.016
3809.956670	0.858	0.021	3981.165439	0.962	0.017	4224.103068	0.809	0.015	4264.300686	0.387	0.022
3809.964112	0.862	0.019	3981.985606	0.741	0.017	4224.970207	-0.663	0.014	4264.303672	0.370	0.020
3817.033236	-0.456	0.019	3982.142591	0.471	0.018	4224.973424	-0.662	0.015	4269.304036	-1.287	0.017
3817.041025	-0.446	0.017	3982.145982	0.459	0.018	4225.093699	-0.856	0.016			
3818.138111	1.125	0.018	3982.947749	-0.871	0.014	4225.096882	-0.881	0.013			
3818.143388	1.120	0.019	3985.289135	1.127	0.015	4225.220674	-1.064	0.012			

Table C.2: RV measurements for α Ari during September 2004 and October 2008

JD-2 450 000 day	ΔRV $m\,s^{-1}$	$\pm\sigma$ $m\,s^{-1}$	JD-2 450 000 day	ΔRV $m\,s^{-1}$	$\pm\sigma$ $m\,s^{-1}$	JD-2 450 000 day	ΔRV $m\,s^{-1}$	$\pm\sigma$ $m\,s^{-1}$	JD-2 450 000 day	ΔRV $m\,s^{-1}$	$\pm\sigma$ $m\,s^{-1}$
3253.283117	-5.0	8.5	4448.032980	-16.9	11.2	4505.938118	13.1	6.1	4718.302818	-49.4	7.9
3253.286219	-18.0	8.5	4448.041961	-7.8	10.9	4505.940664	6.1	5.8	4718.317507	-37.6	9.7
3301.220892	40.3	5.8	4451.905980	-35.4	6.9	4505.943187	17.4	5.9	4719.077853	-56.6	7.7
3301.224485	33.8	6.6	4451.914567	-25.2	7.9	4505.945733	15.4	6.5	4719.081522	-57.3	7.1
3301.227981	34.4	5.1	4451.918051	-32.6	7.8	4506.019591	10.4	6.6	4719.085249	-63.7	7.6
3303.241046	13.0	5.9	4451.929387	-35.9	8.0	4506.022797	6.6	5.9	4719.089115	-47.8	8.2
3303.244495	19.7	4.8	4451.934288	-38.4	6.6	4506.026003	8.1	6.3	4719.092784	-60.9	7.0
3303.247933	17.2	5.3	4453.063429	-6.4	8.0	4506.029289	4.4	6.5	4719.157743	-54.6	8.1
3332.161671	47.5	4.9	4453.067213	-16.3	6.7	4506.032495	14.2	6.7	4719.161239	-58.1	7.5
3332.165235	46.6	5.4	4453.071298	-4.3	6.7	4506.894738	-39.7	8.1	4719.164908	-46.3	8.5
3354.019442	33.2	5.7	4453.099965	-2.7	6.4	4506.896902	-42.1	8.1	4719.168577	-50.2	7.5
3354.023285	37.3	5.0	4453.103171	-4.0	6.5	4506.899413	-27.6	9.7	4719.172246	-52.8	7.5
3354.027474	31.7	4.3	4453.106377	-3.9	6.3	4506.902272	-34.2	7.5	4719.242981	-50.8	8.1
3354.032069	38.2	5.0	4453.109652	3.7	6.4	4506.905478	-38.5	7.0	4719.246476	-42.7	6.5
3356.018152	48.0	5.0	4453.891642	-47.4	8.5	4506.941736	-27.0	8.9	4719.250204	-44.4	7.2
3356.022029	49.7	4.9	4453.894176	-42.4	6.6	4506.947372	-32.8	10.7	4719.253873	-44.7	7.6
3395.018320	66.1	6.4	4453.904939	-46.6	5.5	4506.954049	-35.8	9.9	4719.257542	-44.6	8.3
3395.023111	53.4	7.0	4454.039003	-59.4	6.3	4506.961421	-34.5	9.8	4719.340800	-43.4	7.6
3432.937045	72.1	5.9	4454.040496	-63.0	8.2	4506.968793	-33.9	9.5	4719.344088	-38.8	7.4
3432.941582	76.0	5.7	4454.099404	-50.8	5.8	4506.976200	-13.9	9.6	4719.347178	-40.8	7.5
3760.986427	69.0	4.8	4454.101047	-42.2	5.9	4506.983688	-22.7	8.7	4719.350269	-36.2	7.6
3760.990466	71.3	4.7	4454.104612	-43.0	5.9	4617.324045	50.4	19.8	4726.161139	-50.6	8.3
3779.945100	91.6	5.4	4454.881636	-23.8	5.8	4629.290078	7.8	5.4	4726.164226	-51.3	8.0
3779.949497	89.3	4.6	4454.883568	-16.4	6.9	4629.292358	9.7	5.2	4726.167372	-54.7	8.1
4027.130717	-21.9	5.3	4454.885212	-22.5	5.9	4629.294233	10.3	5.5	4726.253372	-66.9	8.9
4111.049101	44.0	4.9	4454.887075	-21.6	6.0	4629.296108	5.3	5.2	4726.256342	-75.0	8.8
4123.047877	-0.6	5.6	4454.888950	-19.1	5.7	4629.297983	6.2	5.4	4726.259316	-63.5	8.6
4126.048679	48.7	5.2	4454.914284	-19.9	5.9	4629.299859	7.9	5.6	4726.262303	-78.4	8.5
4147.938706	72.7	5.2	4467.903201	-11.6	6.3	4629.301734	3.1	5.3	4726.355959	-77.5	8.3
4165.917523	83.9	6.4	4467.905284	-13.3	6.1	4629.303620	5.3	5.2	4726.359439	-75.3	7.7
4165.920798	73.0	5.1	4467.921093	-24.1	6.2	4629.305727	0.9	5.4	4726.362784	-76.9	8.3
4166.925233	74.7	5.2	4467.923269	-18.4	6.1	4629.307602	3.1	5.3	4736.070261	-52.5	7.5
4262.316527	12.9	6.4	4467.943012	-20.6	6.0	4629.309477	3.7	5.1	4736.074289	-53.5	8.0

Table C.2: continued.

JD-2 450 000 day	ΔRV $m\,s^{-1}$	$\pm\sigma$ $m\,s^{-1}$	JD-2 450 000 day	ΔRV $m\,s^{-1}$	$\pm\sigma$ $m\,s^{-1}$	JD-2 450 000 day	ΔRV $m\,s^{-1}$	$\pm\sigma$ $m\,s^{-1}$	JD-2 450 000 day	ΔRV $m\,s^{-1}$	$\pm\sigma$ $m\,s^{-1}$
4262.318367	7.6	6.3	4467.945524	-22.8	5.9	4629.311422	5.3	5.4	4736.078664	-65.1	9.2
4264.314284	-2.4	6.2	4467.948035	-24.3	5.7	4630.288003	-0.2	6.0	4736.083722	-43.6	12.7
4264.317166	-6.2	6.4	4467.950546	-24.3	6.2	4630.289889	-0.2	5.9	4736.089602	-52.2	8.8
4264.319701	-14.4	6.8	4467.953058	-28.0	6.1	4630.291765	-6.3	5.6	4736.163067	-81.0	8.1
4382.085744	-57.1	6.8	4482.961705	-23.4	6.3	4630.293663	1.4	5.8	4736.166400	-86.5	9.2
4382.090397	-54.9	6.5	4482.968533	-17.1	6.0	4630.295550	-2.9	5.5	4736.169722	-76.8	7.8
4382.127134	-56.9	6.1	4482.974516	-33.9	7.0	4630.297436	-0.5	5.8	4736.173044	-70.1	8.7
4382.173814	-62.0	6.5	4482.980199	-19.8	5.8	4630.299311	-0.3	6.3	4736.176539	-75.6	7.6
4382.235147	-52.2	7.7	4482.986182	-24.4	8.5	4630.301187	-2.7	5.9	4736.350646	-50.9	11.7
4382.269431	-62.3	6.6	4483.052356	-22.9	7.7	4630.303062	-5.6	5.5	4736.356086	-56.0	7.0
4382.310648	-40.9	6.1	4483.058409	-1.7	6.4	4630.305122	-1.7	5.8	4736.361920	-50.9	7.8
4382.357073	-33.7	6.1	4483.065144	-4.0	6.4	4630.307483	-0.0	5.9	4736.367776	-48.5	8.6
4388.018964	-70.8	7.2	4483.070468	-3.4	6.0	4631.291196	2.6	6.9	4737.092883	-84.8	7.4
4388.085564	-73.7	7.0	4483.079113	-2.5	5.7	4631.293406	-1.5	6.6	4737.096151	-86.5	8.9
4388.164131	-68.0	6.7	4483.081994	-6.2	5.6	4631.295548	3.5	5.9	4737.099435	-79.3	7.5
4388.270604	-54.3	6.1	4483.883641	25.1	7.1	4631.298025	-5.7	6.7	4737.102701	-77.3	7.5
4389.276637	-67.6	6.1	4483.886881	8.5	5.5	4631.301208	1.3	7.0	4737.105931	-77.3	7.6
4389.353977	-81.1	6.2	4483.890098	19.9	6.1	4631.304379	11.9	6.5	4737.158200	-73.8	7.6
4389.992881	-61.3	6.6	4483.893327	17.6	7.8	4631.308257	7.0	7.1	4737.161498	-75.7	7.5
4390.036601	-59.2	6.2	4483.896926	-0.7	7.7	4640.260519	-19.3	6.0	4737.164878	-62.1	10.4
4390.116657	-65.4	7.0	4483.901544	10.6	6.1	4640.263100	-15.6	6.4	4737.171603	-72.3	7.2
4390.153626	-67.7	6.0	4483.907978	4.6	5.4	4640.265681	-13.9	6.3	4737.176418	-66.8	8.2
4390.195235	-60.2	6.1	4483.915397	6.3	6.1	4640.268262	-12.7	6.2	4739.210930	-91.7	8.0
4390.222690	-60.5	6.0	4483.922213	13.9	6.6	4640.268262	-15.6	6.3	4739.214263	-79.0	8.4
4390.259450	-56.6	5.8	4483.927143	6.2	6.0	4640.273413	-13.6	6.2	4739.217585	-76.0	8.3
4390.283351	-66.8	6.4	4483.933126	3.7	6.0	4640.275994	-16.2	6.1	4750.999166	-38.9	8.7
4390.308074	-58.7	5.8	4483.939110	2.0	5.8	4640.278576	-18.1	5.7	4751.002673	-44.3	8.1
4390.331072	-66.7	6.1	4483.945093	6.3	5.2	4640.281157	-22.0	5.9	4751.048855	-49.4	8.0
4390.353920	-64.9	6.4	4483.950382	7.9	6.9	4640.283738	-13.7	6.5	4751.052535	-52.6	8.4
4393.025469	-72.2	6.5	4483.955705	-4.1	6.7	4648.258494	-29.4	6.5	4751.056251	-53.3	8.2
4420.109029	-34.7	5.9	4483.961688	5.0	6.9	4648.261064	-36.1	7.4	4751.059932	-55.9	8.2
4420.111077	-28.8	5.8	4483.968366	-7.8	8.0	4648.263633	-30.5	7.4	4751.131890	-68.5	7.5
4420.112929	-32.7	6.2	4504.933956	-13.8	9.4	4648.266203	-28.2	7.4	4751.135223	-62.9	8.3
4420.167279	-33.2	9.0	4504.937162	-25.5	7.2	4648.268773	-23.8	8.8	4751.138730	-56.9	7.9

Table C.2: continued.

JD-2 450 000 day	ΔRV $m\,s^{-1}$	$\pm\sigma$ $m\,s^{-1}$	JD-2 450 000 day	ΔRV $m\,s^{-1}$	$\pm\sigma$ $m\,s^{-1}$	JD-2 450 000 day	ΔRV $m\,s^{-1}$	$\pm\sigma$ $m\,s^{-1}$	JD-2 450 000 day	ΔRV $m\,s^{-1}$	$\pm\sigma$ $m\,s^{-1}$
4422.933749	-11.5	6.2	4504.941861	-19.7	6.7	4648.283114	-22.5	7.3	4751.142411	-65.2	7.1
4422.935670	-11.4	5.3	4504.945957	-20.6	7.1	4648.285695	-30.5	7.8	4751.218883	-69.1	7.7
4423.127794	-38.5	5.1	4504.949962	-24.9	7.7	4648.288346	-21.7	11.5	4751.222911	-65.4	8.1
4423.129611	-32.0	5.4	4504.954012	-20.9	9.1	4657.217648	4.9	8.7	4751.227738	-70.4	8.0
4423.919712	-24.9	5.2	4505.921904	5.5	6.2	4657.220912	6.3	7.7	4751.232020	-59.1	8.8
4423.921344	-27.0	5.0	4505.924867	16.1	5.5	4657.224188	8.7	10.0	4751.308793	-57.3	8.3
4424.067404	-11.6	5.8	4505.927748	10.5	6.5	4718.288303	-68.3	11.6	4751.314361	-47.7	8.4
4424.069048	-13.3	5.7	4505.930503	19.2	6.0	4718.291544	-41.3	8.7	4751.319083	-39.9	10.4
4447.999209	-15.1	9.2	4505.933014	12.7	6.2	4718.295642	-49.6	8.5			
4448.003016	-26.1	5.6	4505.935595	9.1	6.0	4718.299137	-41.5	8.0			

Appendix D

List of SCI papers using BOES

- **The Lorentz force in atmospheres of CP stars: 56 Arietis** D. Shulyak, O, Kochukhov, G. Valyavin, **B. -C. Lee**, G. Galazutdinov, K. -M. Kim, Inwoo Han, and T. Burlakova
published in Astronomy&Astrophysics 509, A28 (2010)

- **Detection of a Planetary Companion around the giant star γ^1 Leo** Inwoo Han, **B. C. Lee**, K. M. Kim, D. E. Mkrtichian, A. P. Hatzes, and G. Valyavin
published in Astronomy&Astrophysics 509, A24 (2010)

- **Can Sodium Abundances of A-Type Stars Be Reliably Determined from Na I 5890/5896 Lines?** Yoichi Takeda, Dong-Il Kang, Inwoo Han, **Byeong-Cheol Lee**, and Kang-Min Kim
published in Publications of the Astronomical Society of Japan 61, 1165-1178 (2009)

- **Atlas of Vega: 3850–6860 Å** Hyun-Sook Kim, Inwoo Han, G. Valyavin, **Byeong-Cheol Lee**, V. Shimansky, and G. A. Galazutdinov
published in The Publication of the Astronomical Society of the Pacific 121, 1065-1069 (2009)

- **A Massive Substellar Companion to the Massive Giant HD 119445** Masashi Omiya, Hideyuki Izumiura, Inwoo Han, **Byeong-Cheol Lee**, Bun'ei Sato, Eiji Kambe, Kang-Min Kim, Tae Seog Yoon, Michitoshi Yoshida, Seiji Masuda, Eri Toyota, Seitaro Urakawa, and Masahide Takada-Hidai
published in Publications of the Astronomical Society of Japan 61, 825-831 (2009)

- **Raman-Scattered He II λ 6545 in the Young and Compact Planetary Nebula NGC 6790** Eun-Ha Kang, **Byeong-Cheol Lee** and Hee-Won Lee
published in The Astrophysical Journal 695, 542-551 (2009)

- **Rotational Velocities of the Components of 23 Binaries** L. V. Glazunova, A. V. Yushchenko, V. V. Tsymbal, D. E. Mkrtichian, J. J. Lee, Y. W. Kang, G. G. Valyavin and **B.-C. Lee**
published in Astronomical Journal 136, 1736-1745 (2008)

- **Precise Radial Velocities of POLARIS: Detection of Amplitude Growth** **Byeong-Cheol Lee**, David E. Mkrtichian, Inwoo Han, Myeong-Gu Park, and Kang-Min Kim
published in Astronomical Journal 135, 2240-2244 (2008)

- **Spectroscopic monitoring of V1357 Cyg = Cyg X-1 in 2002–2004** E. A. Karitskaya, N. G. Bochkarev, A. V. Bondar, G. A. Galazutdinov, **B. -C. Lee**, F. A. Musaev, A. A. Sapar and V. V. Shimanskii
published in Astronomy Reports 52, 362-378 (2008)

- **The BOES Spectropolarimeter for Zeeman Measurements of Stellar Magnetic Fields** Kang-Min Kim, Inwoo Han, Gennady G. Valyavin, Sergei Plachinda, Jeong Gyun Jang, Be-Ho Jang, Hyeon Cheol Seong, **Byeong-Cheol Lee**, Dong-Il Kang, Byeong-Gon Park, Tae Seog Yoon, and Steven S. Vogt
  published in The Publcations of the Astronomical Society of the Pacific 119, 1052-1062 (2007)

- **The Lorentz force in atmospheres of CP stars: θ Aurigae** D. Shulyak, G. Valyavin, O. Kochukhov, **B.-C. Lee**, G. Galazutdinov, K.-M. Kim, I. Han, T. Burlakova, V. Tsymbal, and D. Lyashko
  published in Astronomy&Astrophysics 464, 1089-1099 (2007)

- **Precise radial velocities with BOES Detection of low-amplitude pulsations in the K-giant α Arietis**
  K. M. Kim, D. E. Mkrtichian, **B.-C. Lee**, Inwoo Han, and A. P. Hatzes *published in Astronomy&Astrophysics 454, 839-844 (2006)*

- **A High-Resolution Spectral Atlas of α Persei from 3810 to 8100 Å Byeong-Cheol Lee**, G. A. Galazutdinov, Inwoo Han, Kang-Min Kim, A. V. Yushchenko, Jungho Kim, V. Tsymbal, and Myeong-Gu Park
  published in The Publcations of the Astronomical Society of the Pacific 118, 636-641 (2006)

- **Microvariability of line profiles in the spectrum of the star ι Her** A. F. Kholtygin, G. A. Galazutdinov, T. E. Burlakova, G. G. Valyavin, S. N. Fabrika, and **B. -C. Lee**
  published in Astronomy Reports 50, 220-231 (2006)

- **On the diffuse bands related to the C_2 interstellar molecule** G. A. Galazutdinov, P. Gnacinski, Inwoo Han, **Byeong-Cheol Lee**, Kang-Min Kim, and J. Kreowski
  published in Astronomy&Astrophysics 447, 589-595 (2006)

보현산천문대 고분산에셀분광기를 이용한 거성과 초거성의 고분산 분광 연구: 외계행성탐색, 항성진동학 및 분광선지도

이병철

경북대학교 대학원 천문대기과학과
(지도교수 박명구, 한인우)

(초록)

보현산천문대 고분산에셀분광기 (Bohyunsan Observatory Echelle Spectrograph; BOES)를 이용해서 거성과 초거성의 정밀시선속도를 측정하고 분광선지도를 제작하였다. 이 연구를 위하여 우리는 보현산천문대의 1.8 미터 망원경으로 2003년부터 2010년까지 분광관측을 수행하였다. 분광선지도 제작을 위하여 F-형 초거성 α Persei, 그리고 정밀시선속도 측정을 위하여 F-형 초거성 북극성과 K-형 거성 α Arietis를 선정하였다.

α Persei (HD 20902; F5 Ib)의 분광선지도 제작을 위해서 우리는 Kurucz 분석방법과 관측자료를 기반으로 각 분광선을 동정하고 항성대기모형의 물리량을 구하였다. 결정된 물리량은 $T_{\rm eff}$ = 6240 $\pm$ 20 K, log g = 0.58 $\pm$ 0.04, $v_{\rm micro}$ = 3.20 $\pm$ 0.05 km s^{-1}, 그리고 [Fe/H] = – 0.28 $\pm$ 0.06 이다. 또한 이를 이용하여 합성 분광선지도를 제작하고 완성된 결과는 디지털 자료로 만들고 인터넷에 공개하였다.

북극성 (HD 8890; F7 Ib)은 지난 100 여 년 동안 진동속도가 감소하는 것으로 관측되어 왔으며, 21세기 초에는 진동이 정지할 것으로 예상되었다. 우리는 2004년부터 2007년까지 모두 260 여 장의 분광자료를 획득하고 분석하여 정밀시선속도 및 진동주기를 구하였다. 이 기간의 단기 변화를 보기 위하여 전체 관측기간을 세 시점으로 분할하였다. 진동속도는 2005.183, 2006.360, 그리고 2007.349 시점에서 각각 2K = 2.210 $\pm$ 0.048 km s^{-1}, 2.080 $\pm$ 0.042 km s^{-1}, 그리고 2.406 $\pm$ 0.018 km s^{-1} 로 예상

과는 반대로 급격하게 증가하였다. 이것은 세페이드에서 진동속도가 감소에서 증가로 역전되는 최초의 발견이다. 또한, 작은 진폭 (K $\sim$ 138 m s^{-1})을 가지는 약 119일의 2차 주기를 발견하였다. 이는 1980년대부터 1990년대까지 보고된 34 – 45일의 주기들과는 많은 차이를 보인다. 이러한 원인은 북극성의 자전 ($\sim$ 119일)과 항성표면에서의 비균질성 (흑점의 변화)에 의한 영향으로 짐작된다. 북극성의 진동주기는 이전과 같이 서서히 증가하는 것으로 관측되었다.

여러 가지 단주기 진동이 발견된 K-형 거성 α Arietis (HD 12929; K2 III)의 장주기 변화를 알아보기 위하여 우리는 2003년부터 2008년까지 530 여 장의 분광자료를 얻어서 정밀시선속도를 계산한 결과, 작은 진폭 (K = 65 m s^{-1})을 가지는 395일의 시선속도 주기변화를 찾았다. 이러한 주요 원인으로는 맥동, 자전, 혹은 외계행성의 영향 등 세 가지를 예상할 수 있다. 우리는 395일 주기변화의 원인을 밝히기 위하여 몇 가지 점검을 하였다. 첫 번째, 채층 활동성 지표인 Hα와 CaII 8662Å에 대한 등가폭 변화, 두 번째, Hipparcos 측광자료를 이용한 변광, 마지막으로, 항성표면의 비균질성과 자전에 의한 분광 이등분선 (line bisector) 변화를 확인하였다. Hα와 CaII 8662Å에 대한 등가폭 변화와 변광자료는 시선속도와의 연관성이 전혀 발견되지 않았다. 하지만, 분광 이등분선은 시선속도와 연관성이 일부 발견되었다. 따라서 현재 자료로는 395일 주기변화의 정확한 원인을 규명하기는 어렵지만 두 가지의 설명은 가능하다. 먼저 항성표면의 비균질성 (흑점의 변화)과 자전에 의한 영향이거나, 외계행성에 의한 것으로 볼 수 있다. 혹은, 두 가지의 혼합된 결과로도 볼 수 있다. 만약, 외계행성이라면 최소질량이 2.8–7.2 M_J, 항성에서의 거리는 1.2–1.9 AU로, α Arietis는 지금까지 발견된 가장 크고 무거운 항성중에서 (1.4–5.6 $M_\odot$, 13.9 $\pm$ 0.3 $R_\odot$) 발견되는 외계행성으로 기록될 것이다. 하지만, 명확한 설명을 위해서는 앞으로 추가적인 관측자료가 필요하다.